A Comprehensive Review of Mitigation Strategies to Address Insulation Challenges within High Voltage, High Power Density (U)WBG Power Module Packages

Pujan Adhikari, *Graduate Student Member, IEEE*, Mona Ghassemi, *Senior Member, IEEE*

***Abstract*— Within the expanding domain of electrical power demand, the future of power module packaging is entwined with the progress of (ultra) wide bandgap (UWBG) materials. These materials, like silicon carbide (SiC), aluminum nitride (AlN), and diamond, offer advantages with higher power density, decreased weight, and expanded operational abilities regarding temperature, voltage, and frequency. However, the pursuit of pushing these limits confronts challenges within insulation systems, which may struggle to endure the demands of these parameters, potentially resulting in unfavorable conditions like high electric field, space charge accumulation, electrical treeing, and partial discharge (PD), leading to insulation failure. The emphasis of this paper is to review the insulation challenges within (U)WBG power modules and recent research in mitigating the electric field stress at triple points (TPs) and resolving the PD issues. The manuscript first discusses the high electric field stress issue at triple points. Then, ceramic substrate materials, encapsulation materials, and the influence of harsh weather conditions on them are reviewed. The space charge, electrical treeing, and PD issues within encapsulation materials are analyzed under practical operation conditions of (U)WBG power modules like high frequency, temperature, and square wave pulses. Finally, the various strategies to alleviate the associated insulation challenges are meticulously discussed. While the identified mitigation strategies are able to strengthen insulation systems for packaging, their validation under actual operational conditions of (U)WBG power modules remains relatively unexplored, representing a potential avenue for further investigation. This review offers a valuable framework by providing the constraints of the current studies and recommendations for the future that can be utilized as a reference point for future research endeavors.**

***Index Terms*—(U)WBG power module packaging, partial discharge, triple points, encapsulation material, electric field stress, high power density, field grading materials, nonlinear field-dependent conductivity layer**

I. INTRODUCTION

A notable shift has emerged in recent times toward embracing more electric and all-electric appliances and clean energy, driven by a resolute pursuit of achieving net zero emissions [1],[2]. This trend amplifies the call for electrical power, inevitably escalating the demand. Yet, as we attempt to increase current levels to meet this escalating need for power, we encounter the challenge of voltage drops and consequent power losses, leading to the only viable solution to operating these apparatuses at higher voltages. Moreover, there is an emerging ambition to reduce the weight and size of the power modules and, subsequently, their cost. Combined, these two ideas introduce the concept of high voltage correlated with high power density [3].

However, this ascent into higher voltage and power density territories necessitates innovative approaches to power modules. Here, power modules based on WBG (Wide Bandgap) materials, such as SiC and GaN, and UWBG (Ultra-Wide Bandgap) materials like diamond, AlN, and h-BN stand out as promising solutions [4],[5], which boast higher blocking voltages and superior operational properties compared to traditional silicon-based counterparts, as shown in Fig.1 and Table I. The significance of these materials lies in their ability to thrive under high slew rates (dv/dt) and handle high-frequency repetitive voltage pulses, underscoring their potential in the power domain. Yet, this leap into compact-sized power modules operating at high-frequency voltages has its challenges, as the heightened electric field stress accompanying this operational landscape poses a significant threat to insulation systems within these modules [6].

Two components: ceramic substrates, which electrically insulate the chips while dissipating generated heat, and encapsulation materials, shielding vital elements from moisture, dirt, and vibrations, constitute the essence of insulation systems in power electronics modules. The electric field stress surge raises concerns about potential partial discharges (PD), accelerated aging, and ultimately, premature

This paragraph of the first footnote will contain the date on which you submitted your paper for review, which is populated by IEEE. This work was supported in part by the National Science Foundation (NSF) under Award 2306093. *(Corresponding author: M. Ghassemi).*

The authors are with the Zero Emission, Realization of Optimized Energy Systems (ZEROES) Laboratory, Department of Electrical and Computer Engineering, The University of Texas at Dallas, Richardson, TX 75080 USA (e-mails: pujan.adhikari@utdallas.edu; mona.ghassemi@ utdallas.edu).

Color versions of one or more of the figures in this article are available online at http://ieeexplore.ieee.org

Table I: Comparison of properties of conventional (Si), WBG (SiC, GaN), and (U)WBG materials [7] [8]

Parameter	Unit	Si	SiC	GaN	AlN	h-BN	Ga_2O_3	Diamond
Bandgap	eV	1.1	3.0-3.4	3.4-3.6	6	6.1	4.9	5.45
Critical electric field	kV/mm	30	300	330	1540	700	1000	1300
Thermal conductivity	W/m-K	150-200	300-490	100-150	319	550±75	27	2200
Breakdown voltage	kV	0.6	10	1.2	>10	>10	>10	>10
Dielectric constant		11.9	9.66-10.1	9	9.76	5.7	10	5.5
CTE	(*10^{-6} /°K)	2.6	3.8-4.2	5.6	4.5	2.0	6.5	1-2

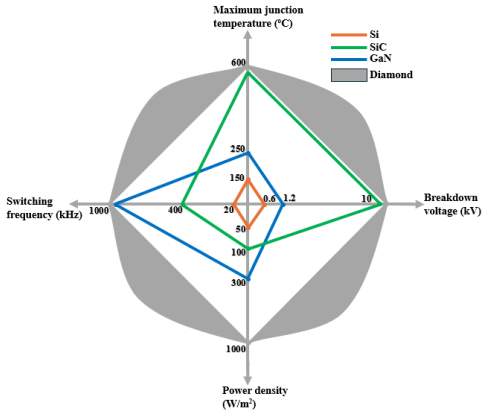

Fig 1. Graphical representation of properties of conventional and (U)WBG materials for power modules packaging

insulation failure within the power module [9][10][11].

Fig. 2(a) illustrates a general schematic of a metalized ceramic substrate for high voltage, high power density (U)WBG power module packaging. The metallization layers are soldered into the ceramic substrate (e.g., aluminum nitride), either through active metal brazing (AMB) or direct bonded copper (DBC) technology, and are encapsulated with packaging materials (e.g., silicone gel) [12]. The triple point (TP) formed at the interface of metal electrodes, substrate, and encapsulation material, the protrusions on metal edges and voids or cavities within the encapsulant, all introduce intolerable electric, thermal, and mechanical stress within the power module, which may cause the breakdown of the insulation. Thus, extensive attention has been devoted to mitigating this electric field stress and bolstering the partial discharge inception voltage (PDIV) of insulation materials within the system [13], [14], [15].

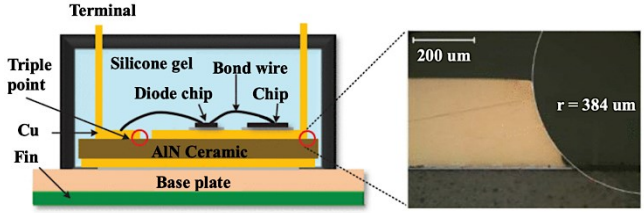

Fig. 2. (a) Schematic of an IGBT/diode showing protrusion and triple points [12].

Complicating matters further is the exposure of insulation materials to temperatures surpassing their capacity due to the operational demands of WBG power electronics modules [16], [17]. It has been suggested that (U)WBG power modules involving aluminum nitride (AlN) and diamond can operate for temperatures exceeding 500°C, but their performance will be limited by present insulation materials having a maximum operating temperature below 200°C. This heightened temperature exacerbates the likelihood of insulation damage, an area that has unfortunately received limited attention in existing literature. While thermal conductivity (TC) has historically served as the primary criterion for assessing the suitability of a polymer as a packaging material, it's become evident that a more holistic evaluation, considering properties like coefficient of thermal expansion (CTE), glass transition temperature (T_g), and thermal degradation temperature is imperative for assessing the thermal performance of insulation systems [18].

This comprehensive review explores the multifaceted challenges posed by high electric field stress and PD within the insulation systems of power modules. It meticulously examines the impact of temperature and frequency on electric field stress at TPs and PDIV while studying various mitigation strategies to combat these issues. The paper is divided into six sections: section II analyzes the necessity of considering the electric field evaluation at TP, and section III discusses the ceramic substrate, encapsulation materials, and the effect of harsh weather conditions on their properties. Section IV is dedicated to the space charge, electrical treeing, and PD analysis of encapsulation materials under practical power module operational conditions. Section V reviews the mitigation strategies undertaken so far to attain the desired goals of electric field mitigation and PD control, their significance, and their limitations. Finally, Sections VI and VII conclude the paper by evaluating the success of the research conducted so far, the challenges currently faced, research gaps, and future recommendations. Proposed recommendations urge a shift towards improving PDIV and reducing electric field stress under actual operational conditions of (U)WBG power modules- specifically focusing on high frequency and temperature scenarios and exploring alternative polymers to replace silicone gel as encapsulation material remains an area for exploration, warranting the examination of recent papers not covered in prior reviews. In essence, this comprehensive analysis ventures beyond the confines of previous studies [19], [20] to evaluate the nuances of power module packaging, centering its focus on the critical insulation properties that underpin the integrity and performance of these systems.

II. Triple Points and Their Electric Field Evaluation

As shown in Fig. 2(a), triple points (TPs) emerge at the meeting point of the encapsulation material, ceramic substrate, and metal electrodes. These TPs pose a significant challenge in power electronics module packaging, as they experience maximum electric field intensity, compounded by the interface

between the encapsulant and substrate, which acts as a vulnerable area for insulation [21], [22], [23]. This is because the dielectric properties are vastly different for a polymeric encapsulant from a ceramic substrate, and therefore, the interface comes across an abrupt change in dielectric values. One prime example is CTE mismatch due to different CTE between various components within the power module, resulting in thermomechanical stress and leading to pre-mature insulation failure and breakdown [24], [25].

Commonly available materials exhibit distinct electrical conductivities, ranging from 10^{-11} to 10^{-13} S/m for substrates and 10^{-13} to 10^{-15} S/m for encapsulants, with their relative permittivity being highly different (approximately 9 and 2.8 for AlN substrate and SG, respectively). Furthermore, surface imperfections, like protrusions or sharp edges on the ceramic substrate due to imperfect metallic substrate fabrication, as well as the presence of pores and air-filled voids or cavities within encapsulation materials, escalate the electric field stress at TPs and the electrical treeing propagation process. Elevated electric field values at TPs often trigger PD activity in the encapsulation material, which generally exhibits lower dielectric strength than the substrate. This phenomenon results in the formation of electrical trees, ultimately contributing to insulation aging and dielectric breakdown [26]. These challenges become particularly pronounced in insulating packaging for (U)WBG power modules, given their requirement to function optimally under high frequency, rapid slew rates, varying temperatures, and low-pressure conditions, especially in harsh weather environments [27]. Consequently, numerous studies have been undertaken to analyze the electric field and PD issues at TPs, aiming to resolve these concerns to ensure the reliable operation of high voltage, high power density (U)WBG power modules.

Calculating the electric field at TPs within power modules through experimental investigations is complicated. And for this reason, the finite element method (FEM) analysis is carried out to observe the electric field distribution with the help of software tools like ANSYS and COMSOL Multiphysics [28].

The TP is a singularity point with an infinite electric field; the field calculation is done at an appropriate distance away from TP in such a way that the accuracy of the electric field calculation isn't compromised. In the study [29], AlN substrate with an electrical conductivity of $1.72\text{x}10^{-11}$ S/m and relative permittivity of 9 and SG encapsulant with electrical conductivity of 10^{-11} S/m and relative permittivity of 2.7 were used for simulation. The electric field distribution was observed, and as shown in Fig. 3, the electric field value at TP was 65.34 kV/mm, 211% higher than the dielectric field strength of 21 kV/mm.

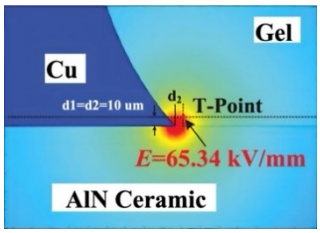

Fig.3. Electric field distribution around Triple point [29].

Various studies have confirmed that the electric field tends to differ among different TPs within a power module, and the value is exceptionally prominent around the encapsulation region due to its inferior dielectric characteristics and lower dielectric strength. Z. Huang et al. [15] observed the electric field to be 23.2 kV/mm, 18.2 kV/mm, 17.3 kV/mm, and 21.2 kV/mm at four different measuring points - P1, P2, P3, and P4, respectively, shown in Fig. 4. These points were located just 50 μm from the TP, with P1 being at the SG and near the HV electrode, P2 at the Al_2O_3 substrate and near the HV electrode, P3 at the Al_2O_3 substrate and near the ground electrode, and P4 at the SG and near the ground electrode. This finding is particularly significant as it highlights that the electric field around the HV electrode's TP is higher than the ground electrode and higher in the SG region than the Al_2O_3 substrate. As a result, most of the research in this area is focused on mitigating the electric field stress at the TP around the encapsulation region near the HV electrode.

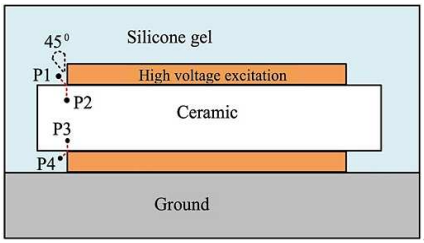

Fig. 4. Diagram illustrating the location of 4 TPs within the power module [15]

III. Insulation Materials

A. Ceramic substrate materials

In power module packaging, the ceramic substrate serves two main purposes. The first function is to provide electrical insulation to the electronic circuit, which primarily hosts the active semiconductor device(s), and the second function is to enable the removal of heat generated by power losses within the active devices. The first role demands the ceramic substrate material to have good dielectric properties in terms of dielectric constant, loss factor, dielectric breakdown strength, and electrical conductivity, meanwhile, it also needs to have desired thermal properties in terms of TC, thermal diffusivity, and CTE. Considering the function of ceramic substrate to functionally bind the entire components within the power module, it is additionally expected to possess high mechanical stability in terms of bending strength, Young's modulus, and fracture toughness. The properties that determine the reliable performance of the ceramic substrate material in (U)WBG power modules are presented in Table II.

The two widely used ceramic substrate materials in WBG power modules currently are Al_2O_3 and AlN. However, Al_2O_3 suffers from poor TC and mechanical strength despite having the lowest cost among all the substrate materials. AlN, on the other hand, has better dielectric and thermal properties than Al_2O_3, even though the cost is high. However, as the research on (U)WBG materials is significantly progressing, the poor mechanical characteristics of AlN substrate (fracture toughness, bending strength, and CTE) restrict its utilization in next-

generation power modules. Additionally, as pointed out in [30], the TC of AlN keeps on decreasing with temperature, reaching as low as 110 W/m-K when temperature reaches 300ºC. Experiments have shown that AlN and Al_2O_3 substrates aren't able to withstand more than 500 thermal cycles. Hirao et.al. [31] discovered that only 55 cycles are enough to cause failure of power module for DBC Al_2O_3 substrate and less than 100 cycles lead to either formation of cracks on metal-substrate interface or complete failure of the insulation system in AlN substrate. Meanwhile, even with more than 3000 cycles of thermal testing at 250ºC, Si_3N_4 showed no delamination or interfacial cracks. Similar results were obtained in [32] where AlN substrate showed crack formation within 50 thermal cycles whereas Si_3N_4 was able to endure more than 1000 cycles without crack formation under ASM imaging. Where the residual strength of AlN substrate was only 0.51 times original bending strength, the ratio was 0.86 after 10 cycles and 0.76 after 1000 cycles for Si_3N_4. These experimental investigations validate the stability of Si_3N_4 substrate compared to AlN and Al_2O_3 due to its high bending strength, fracture toughness, and lower CTE.

Table II: Electrical, thermal, and mechanical properties of ceramic substrate materials [33] [34]

Substrate material	Al_2O_3	AlN	BeO	Si_3N_4
Dielectric constant	9-10	8-9	6-8	8-9
Resistivity (Ω-m)	$>10^{12}$	$>10^{12}$	$>10^{12}$	$>10^{12}$
Loss factor	3×10^{-4}-1×10^{-3}	3×10^{-4}	3×10^{-4}	2×10^{-4}
Dielectric breakdown strength (kV/mm)	10-35	14-35	27-31	10-25
Thermal conductivity (W/m-K)	20-30	120-200	209-330	40-100
CTE (ppm/K)	7-9	4.2-7	7-8.5	2.7-4.5
Bending strength (MPa)	300-380	250-350	≥250	600-900
Fracture toughness ($MPa.m^{1/2}$)	3-5	2-3	1-2.5	4-7
Young's modulus (GPa)	300-370	300-320	330-400	200-300
Reliability (number of cycles)	300	200	/	≥500

Clearly, from Table II, it can be observed that Si_3N_4 has the best properties for a ceramic substrate when we compare the characteristics holistically. The two primary issues with commercial Si_3N_4 materials are their cost and slightly lower TC values than AlN substrates. Therefore, Si_3N_4 can be used as a better alternative to AlN if its TC can be increased without compromising its mechanical characteristics. One way that can be achieved is by sintering Si_3N_4 materials with additives at high temperatures under nitrogen pressure. The changes in TC, flexural (bending strength), and fracture toughness with some of the studies have been reviewed and presented in table III.

In recent years, it has been suggested that non-oxide sintering additives are better at improving the TC and fracture toughness of Si_3N_4 materials. This is because oxygen has been established as the principal impurity in Si_3N_4 lattices, as it causes phonon scattering, which decreases the phonon-free path, thereby reducing TC. Therefore, removal of oxygen from lattices becomes the primary criterion. This has been validated by Zhu. et.al. [35], where 5% $MgSiN_2$-2% Yb_2O_3 additive increased the TC of pure Si_3N_4 ceramic to 113 W/m-K and fracture toughness to 10 $MPam^{1/2}$ compared to 97 W/m-K and 8 $MPam^{1/2}$ with 5% MgO-2% Yb_2O_3 additive.

Hu et.al. [36] discovered that even though Si_3N_4 with 7 mol% $MgSiN_2$ additives had 9.6% higher bending strength, its TC and fracture toughness were 8% and 9.4% lower while also having 437% higher dielectric losses than 5 mol% $MgSiN_2$ additives. This has also been validated in [32], where Si_3N_4 with 3 mol % ZrSi2- 4 mol % MgO had the best TC and flexural strength, both of which were reduced for Si_3N_4 with 3 mol % ZrSi2- 4 mol % MgO. Therefore, a balance must be maintained with the ratio of sintering additives. In the comparison of commercial Si_3N_4 materials [37], it was observed that despite having higher initial flexural strength, its value reduced to less than 400 after 1000 thermal cycles while SN-1 was able to maintain its flexural strength. This investigation highlighted that the thermal-shock resistance of a substrate or thermo-mechanical stability depends on fracture toughness of the substrate rather than initial bending/flexural/tensile strength, as the fracture toughness of the material which was able to retain its mechanical properties almost twice the fracture toughness as the other one.

The parameters on which the properties of Si_3N_4 depend are the sintering temperature and holding time in addition to the size, ratio, and type of sintering additives [38]. When the sintering temperature and holding time are increased, it has the effect of promoting the growth of b-Si3N4 grains. Additionally, the crystal lattice's oxygen content is continuously lowered by the dissolving-precipitate process, which in turn enhances the thermal and dielectric properties. However, for thinner thickness, this leads to lower breakdown strength decreasing from 99.5 kV/mm to 9.8 kV/mm only when sintering period was increased from 6 hours to 48 hours [38]. Additionally, impurities interfere with the additive/substrate interface leading to the formation of cracks, and defects and drastically reduce the properties of Si_3N_4. The higher the impurity content, the higher will be the deterioration of electrical, thermal, and mechanical properties. The fracture toughness, TC, and bending strength of 2 mol% Y_2O_3/ 5% MgO was reduced to 6.5 $MPam^{1/2}$ and 53 W/m-K only with 5% iron impurity, as seen from [39]. The primary challenge in implementing Si3N4 as a ceramic substrate in (U)WBG power modules lies in finding cost-effective ways to create high-thermal-conductivity silicon nitride ceramics [40]. Presently, such ceramics are only produced by subjecting them to extended heat treatment at high temperatures. However, this method is not only expensive, but it also consumes a considerable amount of energy and has long cycle times. Therefore, future studies should concentrate on reducing the sintering temperature and holding time, with a particular focus on regulating the influence of grain boundary phases and lattice oxygen at shorter holding times and lower temperatures. This should enable the production of high-TC silicon nitride ceramics in a more energy-efficient and affordable manner.

B. Encapsulation materials

SG is the most widely used encapsulation material in power module packaging due to its excellent electrical properties, ease of processing, high elasticity, and self-healing properties [41], [42]. It is a two-state dielectric material composed of a mixture

Table III: Properties of Si_3N_4 ceramic with additives on different sintering conditions

Additives on Si_3N_4	Sintering conditions	Thermal conductivity (W/m-K)	Flexural strength (MPa)	Fracture toughness ($MPam^{1/2}$)	References
1 mol% $ZrSi_2$- 6 mol% MgO	12 hours under 1900ºC	89.22	505±50	5.67±0.12	[32]
3 mol % $ZrSi_2$- 4 mol % MgO		113.91	553±39	6.36±0.32	
6 mol % $ZrSi_2$- 1 mol % MgO		94.65	495±60	6.56±0.35	
2 mol % La_2O_3/5 mol % MgO	2 hours under 1900ºC	79.6	733	8.31	[38]
2 mol % Y_2O_3/5 mol % MgO		81.4	758	10.41	
2 mol % Er_2O_3/5 mol % MgO		90	953	10.6	
2 mol % Yb_2O_3/ 5 mol % MgO	12 hours under 1900ºC	97	663	8	[35]
2 mol % Yb_2O_3/ 5 mol % $MgSiN_2$		113	663	10	
3 mol% Y_2O_3/ 5 mol% $MgSiN_2$	3 hours under 1890ºC	91.9	845	8.41	[36]
2 mol% Y_2O_3/ 7 mol% $MgSiN_2$		84.5	926	7.62	
SN-1	/	140	544 >500 (1000 cycles)	10.5±0.2	[37]
SN-3		/	637 <400 (1000 cycles)	5.5±0.1	
2 mol% Y_2O_3/ 5% MgO (SBN)	24 hours under 1400ºC	103	624	/ /	[39]
2 mol% Y_2O_3/ 5% MgO (SRBSN)		154	505	10.63±0.37	
2% Y_2O_3/ 5% MgO (iron impurity %)	6 hours	0.1% - 81	0.1% - 756	0.1% - 7.5	
		5% - 53	5% - 733	5% - 6.5	

of lightly cross-linked silicone elastomer (SE) and silicone liquids, giving it a complex characteristic determined by both phases. J. Wang et al. [43] conducted a study to investigate how temperature and frequency impacted the self-healing properties of SG by considering fractal dimension, expansion coefficient, and duty ratio. The results showed that an SG containing 50% of specific components exhibited the most effective self-healing capability against electrical treeing. However, the study had its limitations as it only utilized a maximum frequency of 18 kHz and a peak investigation temperature of 100°C, which fall short of the thresholds required for (U)WBG power modules. In [43], the dielectric properties of three commercial SGs were analyzed, and it was found that all three gels had a T_g around -120°C, and thermal degradation temperatures exceeding 400°C were exhibited by gels 1 and 3. Furthermore, gel 3 emerged as the most promising material for encapsulation based on various factors, including dielectric loss, breakdown field strength, volume resistivity, and thermal stability. However, it is essential to conduct further investigation into the self-healing abilities of gel 3, given its similarity in adhesion characteristics and electrical treeing morphology to elastomers, which might limit the self-healing ability acquired from its liquid phase.

Epoxy resins (EPs), high-performance thermosetting resins, are another encapsulation material commonly used in power module packaging due to their excellent electrical, thermal, and mechanical properties. It is observed that EPs are desired for power module packaging due to their higher dielectric strength (>20 kV/mm), lower water absorption rate (<0.1%), higher TC (>0.8 W/m-K), and lower CTE (<8/38 ppm/K). However, EPs' lower T_g (<135ºC) hinders their performance below 200ºC. Additionally, the viscosity of EPs (> 50 Pa.s) is significantly higher than SG and the desired limit of high-temperature encapsulant[44], [45]. This hinders the easy flow of the material in power modules, which leads to the formation of voids, bubbles, and defects that accelerate insulation aging. They depict a higher value of Young's modulus than the criterion limit, which adds to the thermo-mechanical stresses the encapsulation material experiences. Therefore, many studies have been carried out to improve the thermal and mechanical properties of EP matrix [46] [47] [48], which will be discussed in detail later.

It has been suggested that harsh weather conditions such as low pressures, cosmic radiation, and moisture accelerate the insulation degradation of encapsulation materials. In [49], Zhang et.al. aimed to assess mass changes, relative humidity variations, and the diffusion coefficient in SGs during moisture absorption or desorption. SG A exhibited significant mass gain during moisture exposure, while SG B displayed a peculiar mass loss over time, prompting speculation about potential volatile additive loss within the SG matrix. Unfortunately, the gravimetric analysis failed to provide conclusive results for the moisture diffusion coefficient, possibly attributed to the observed mass loss. For this, researchers in [50] introduced T_g concept. In the case of EP, the moisture absorption temperature is lower than T_g, emphasizing the dominance of absorption over dissolution in driving mass changes. Conversely, SG, characterized by a negative T_g, exhibits the impact of small molecule dissolution and evaporation within the SG matrix, leading to a noticeable mass loss effect. The intrusion of moisture into the polymer initiated the formation of percolation paths, creating additional channels for discharge within the system. Simultaneously, the presence of moisture caused a distortion in the electric field which, in turn, contributed to a reduction in breakdown strength. The breakdown strength was reduced by 59%, 48% and 57% for AC, DC+, and DC- voltages after 1000 hours of moisture assisted thermal aging. The effect of moisture uptake in EP with different resin/hardener ratio was analyzed and it was observed that 1% water absorption led to 10% reduction in T_g and 35% reduction in DC breakdown strength [51]. Adjusting the resin/hardener ratio alters the crosslink density and chemical composition of the network. Crosslink density influences T_g, network structure, and free volume content, while chemical composition affects the concentration of polar sites (hydroxyl and amine groups). These changes impact water absorption characteristics, as moisture absorption replaces hydrogen bonds, leading to altered polar

concentration and degraded properties. This mechanism also showed 2.34% moisture uptake and 10^{-7} mm^2/s diffusion coefficient in [52] in addition to a reduction in flexural strength of EP from 58.5 MPa to 51.4 MPa, higher CTE, and lower T_g.

The mechanism behind the degradation of SG properties due to thermal aging is the involvement of O_2 due to aging reaction process and the breaking of organic side chain methyl of the SG. As thermal aging progresses, the crosslinked network architecture becomes tidier, and free volume increases. This elevated free volume enables carriers to gain more energy during travel, facilitating easier crossing of the breakdown threshold which leads to breakdown voltage decrease. Simultaneously, high temperatures accelerate surface hardening of SG in full contact with air. This leads to uneven microscopic defects, contributing to lower breakdown field strength in aged samples compared to unaged specimens. This is likely the case in [53] which shows an increase in Si-O-Si bond and a decrease in C=C bond, an increase in element O percentage and a decrease in element C, increase in crosslink density, free volume, and hardness (thus loss of elasticity properties), all of them leading to PDIV decrement. Paper [54] concludes that exposure temperature significantly affects aging conditions, with characteristics deteriorating rapidly after 6 hours, especially beyond T_g. At 50% T_g for 2160 hours, there is only a 0.5% weight loss, but at 145% T_g for 6 hours, the loss exceeds 3%. Flexural and shear strength are maintained at 50% T_g for 2160 hours, with potential property enhancement due to resin curing at lower temperatures. However, at higher temperatures (75% T_g to 145% T_g), significant reductions are observed, linked to structural changes in EP. While the exact mechanism isn't explained, it's attributed to polymer chain scission and thermal oxidation, emphasizing the crucial role of T_g in preserving encapsulant's properties for high-temperature operations. Similar degradation patterns are noted in dielectric properties [55].

Combined UV thermal and hydrolytic aging has more pronounced impact on hardness compared to thermal oxidation aging [56]. UV radiation encourages the formation of Si-OH bonds, while thermal-hydrolytic aging significantly influences the quantity of Si-OH groups. The synergy of UV thermal and hydrolytic aging results in cross-linking reactions and the rupture of Si-O-Si backbone, leading to increased material hardness. This hardness elevation affects the average contact pressure, with a post-aging increase of about 30%, coupled with a 20% reduction in contact area, contributing to heightened stress concentration and a consequent decrease in service life. Similar findings were reported in [57], where SiR dielectric properties exhibited distinct changes for thermal aging, gamma irradiation, and steam aging. Thermal aging primarily involves an increase in crosslinking degree, gamma irradiation leads to carbonyl group (C=O) formation and C=C side bond breakage, while steam aging results in hydroxyl group formation at lower temperatures and an increase in both hydroxyl formation and crosslinking degree at higher temperatures.

When transitioning to all-electric electric aircraft, the impact of pressure on insulation materials becomes crucial, especially considering aviation pressures as low as 4 psi. The influence of low pressures on electric machines has been discussed in [10], where an abrupt fall in breakdown voltage is seen for an air gap between two spherical electrodes with similar negative impacts seen for PDIV for twisted wire pairs and stator winding. Lower pressure leads to higher discharge magnitudes and current density, as explained in [58]. Additionally, the field displacement decreases with lower dielectric constants, affecting true charge magnitude. While ε_r gradually decreases with reduced pressure, the true charge magnitude increases from 600 to 630 pC, and PD duration extends from 0.12 µs to 0.2 µs when pressure drops from atmospheric to 4 psi [59]. This implies that, in low-pressure conditions, later extinction times outweigh the shortening due to later inception times prolonging PD phenomenon and PD magnitude increases, highlighting the detrimental impact of pressure in aviation.

IV. Space Charge, Electrical Treeing, and Partial Discharge Analysis

The operation of the next generation of power modules based on materials like diamond or AlN will constitute high-frequency operation. However, the current encapsulation materials (SG and EP) don't have the capacity to withstand such a high-frequency operation without failure. This is mainly due to the degradation in electrical, thermal, and mechanical properties that high frequencies bring in these encapsulants. Mainly, this degradation can be attributed to space charge accumulation which causes electric field distortion, initiates electrical treeing, and partial discharges, and leads to insulation failure. Additionally, it has been explained that the space charge and electrical treeing characteristics are different under PWM pulses than DC voltage. Therefore, space charge characteristics, electrical treeing, and PD activity within insulation system need to be discussed in detail.

Because of the unconventional insulation arrangement in the power module package, TP experiences the most significant electric field stress. In this area, charges may be introduced from the metallization layers on the ceramic substrate, subsequently gathering in the encapsulation materials surrounding the metallic edges. These accumulated space charges distort the local electric field, consequently influencing the characteristics of PD. A charge dynamics and trap level mechanism was proposed in [60] to explain why pure EPs exhibit higher average space charge amounts at higher temperatures and electric field. It was concluded that the interfacial barrier height that the injected charges from TPs need to surpass is lowered for high temperature and electric field due to electrothermal emissions and tunneling effect, respectively. For EPs, the energy level of the shallow and deep traps are high, which means that de-trapping of the accumulated space charges becomes difficult. This leads to the accumulation of space charges and causes electric field distortion. The space charges under high frequencies not only depend on the type of voltage waveform and its magnitude but also the polarity. Y. Wang et.al. [61] observed that the PDIV of tested samples under square voltage was reduced by 10% and 12% for 0.35 mm and 0.5 mm gap distance compared to DC voltage. This is attributed to the lower space charges accumulation seen under DC voltage in [62]. C. Dai et.al. [62] observed that under positive square voltage pulse, low frequency (50 Hz) has more serious impact than high frequency (500 Hz) and under negative square voltage, high frequency leads to significantly higher

space charge accumulation during polarization and lower space charge dissipation during depolarization. Furthermore, the highest space charge accumulation near the electrodes and in the bulk region between the electrodes is seen for negative square pulse voltage under higher frequency. However, why this discrepancy occurs with different voltage polarity hasn't been discussed. The effect of space charges on electric field distortion under high-frequency operation is exacerbated by the operation of power modules at high temperatures. In [63], it was concluded that higher temperatures reduce the interfacial barrier of encapsulants and increase the injection of charges from electrodes and TPs. Higher temperature also leads to a decrease in trap depth of deep traps and an increase in charge mobility, thereby reducing the surface potential decay (SPD), increasing the electrical conductivity, and reducing the breakdown strength. The combined effect of high temperature and high frequency under different polarities of square wave pulse on space charge characteristics is more evident in [64]. As seen from Fig. 5, the accumulation of space charges is considerbly higher under higher temperatures (80°C > 30°C) and higher frequencies under negative square voltage (which is more severe than positive as described above). This effect is in turn seen in the average charge amount (which indicates the higher space charge accumulation under polarization and lower charge dissipation under depolarization). The average charge amount for EP increases from 3.44 nC to 7.30 nC under 25°C for frequencies of 10 Hz and 500 Hz, respectively. When temperature is increased to 500°C, the average charge amount increases to 13.05 nC and 26.79 nC, respectively.

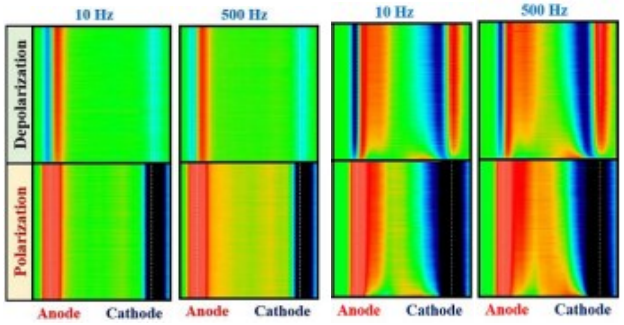

Fig. 5. Diagram depicting space charge accumulation under: (a) 30°C/10 Hz, (b) 30°C/500 Hz, (c) 80°C/10 Hz, (d) 80°C/500 Hz [64]

In a study by S. Nakamura et al. [65], the effect of frequency and rise time on the electrical treeing behavior of SG under repetitive voltage pulses was investigated, shown in Fig. 3(a). The results showed that as the frequency increased from 50 Hz to 1 kHz and the rise time decreased from 120 ns to 110 ns, the tree length in SG increased from 0.7 mm to 2.2 mm, as shown in Fig. 3(b). This was because when the frequency and slew rates are increased, the interval between subsequent PD pulses is shortened, and the next PD pulse reaches the discharge track before its disappearance through the self-healing properties of SG. As shown in Fig. 3(c), this leads to the propagation of the cavity and the growth of electrical trees, which ultimately hampers the performance of (U)WBG power modules below their optimal capacity. This was further supported in a PD analysis through a modeling approach [66, 67]. The authors considered an air-filled cavity in SG between two sphere electrodes and examined that the electric field stress isn't uniformly distributed in the presence of the cavity, concentrating towards the air-filled cavity with a lower dielectric strength, as shown in Fig. 4(c) and 4(d). This is because, compared to the encapsulant, air has a lower dielectric permittivity, and the electric field is directly proportional to the ratio of their ε_r. As SG can have more than one void present, they also investigated the PD activity for two voids of different sizes under the effect of low-pressure conditions [68]. The findings revealed that even though PD only occurs at the 0.3 mm void at atmospheric conditions due to its inception electric field being lower than that of the 0.2 mm void, the inception electric field at P=0.5 atm reduces by 36% and 37% in the 0.2- and 0.3-mm voids, respectively, and breakdown happens at both of these voids. A bubble expansion theory was proposed in [69] to explain the PD phenomenon in SG, where it was suggested that small metal protrusions act as the initiation point of gas bubbles and that the threshold voltage of PD inception would be attained sooner with fast rise times, the bubbles expand in shorter time exacerbating the breakdown process.

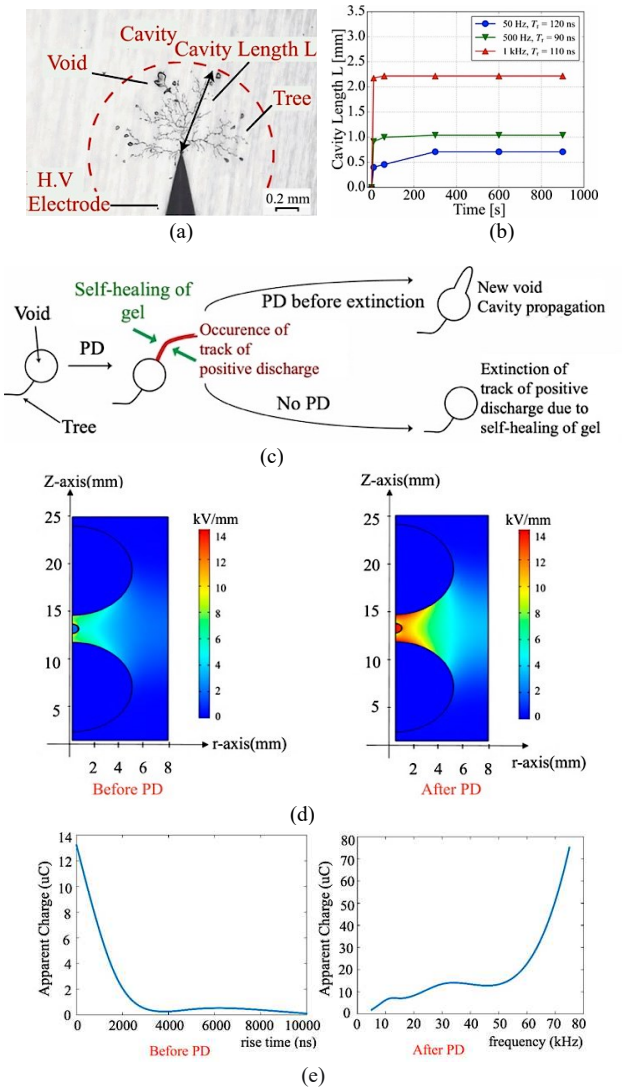

Fig. 6. (a) Electrical tree within encapsulant. (b) Tree lengths for 3 different frequencies and rise times. (c) Cavity propagation process (d) Electric field distribution for void (e) Change in Apparent charge before and after PD [65][66].

In [70], it was observed that the electric tree grows from dendritic to pine branch and jungle-like electric trees for higher frequencies, which grows more densely and in all directions. The fractal coefficient increases by 37% compared to 7.3% within 8 mins when frequency is increased from 8 kHz to 18 kHz. The expansion coefficient first increases and then decreases for high frequency, suggesting that first the tree grows horizontally (sideways) and after reaching a certain length, starts to propagate vertically upward, giving a bush-like structure. The theory used to explain the PD propagation phenomenon aligns with [31]. In [71], it was observed that the tree length is 200-400 µm for 50-500 Hz, 500-700µm for 1-4 kHz and 800-1000µm for 5-10 kHz. Increased frequency means an increase in the number of rising edges per unit time and a decrease in recovery time after every single pulse. Therefore, space charges generated by PD increase due to intensive discharges. The space charges are captured by traps and cause electric field distortion, thus influencing the PD activities.

In an interfacial electrical treeing analysis in [72], the electrical treeing test of both lateral and vertical modules showed that in SE, injected positive charges from anode are de-trapped easily due to shallow traps in polymer matrix, where they generate positive hetero space charge accumulation by migrating towards cathode. The PRPD pattern shows high PD magnitudes to be concentrated around main tree branches, leading to concentration of energy, and thickening of main branches, ultimately resulting in IET breakdown. This effect on PD characteristics is more prominent at higher temperatures, as the PDIV reduced by 35% and average PD density increased by 63% when temperature increased from 30 to 200°C.

B. Zhang et al.[41] conducted a comprehensive analysis of the electrical properties of commercially available SG at higher temperatures (up to 200°C). It was discovered that the volume resistivity of SG decreases by three orders of magnitude, the breakdown strength reduces by 52% and 42% for AC voltage and square voltage, and the dielectric loss is increased by four orders of magnitude corresponding to the increase in the imaginary part of relative permittivity. These changes are due to the increase in charge carriers by high-temperature performance. Y. Lin et al. [73] suggested that the ceramic substrate remains stable during insulation degradation, and attention must be given to the electrical parameters of the SG encapsulant. In their temperature and degradation-dependent electric field analysis, it was discovered that the electric field stress at TP increases by 100% when the temperature rises from 150 to 250°C while simultaneously decreasing the PDIV by 24%. This is attributed to the mismatch of electrical parameters of the insulating materials, specifically the DC conductivity and the relative permittivity of SG. These findings are consistent with the results obtained from [74] which indicated that despite having a lower number of PD pulses, the magnitude is increased by 82% when the temperature is increased from 30 to 110°C. This leads to severe damage to encapsulation as the degradation rate is determined by those PD pulses with a high enough magnitude to deteriorate their cross-linking density. It was concluded that the rise time of square pulses negatively impacts the PDIV, and the impact is more severe under higher temperatures, which is precisely the conditions under which (U)WBG power modules are targeted to work.

As research on (U)WBG power modules advances, it has become apparent that the high CTE of SG causes CTE mismatch and limits the application of power modules to temperatures below 200°C because of thermomechanical instability. Furthermore, the self-healing characteristics of SG have yet to be investigated in temperatures exceeding 200°C. As observed in [41], the dielectric properties of SG deteriorate at high temperatures and pressures, and similar effects might be observed on the self-healing characteristics. Moreover, the high viscosity and low T_g of EP limit its utilization to below 200°C for WBG power module packaging. Space charge analysis shows that high space charge accumulation of EPs under higher temperatures and frequencies leads to electric field distortion and PD inception. Therefore, several research articles have suggested alternative encapsulation materials by adding nanofillers to improve the insulation system's thermal, mechanical, and electrical properties for envisaged (U)WBG power modules. The development of alternative encapsulation materials can provide a solution to the limitations of SG, allowing for the creation of (U)WBG power modules that can operate at higher temperatures, frequency, and power density.

V. Mitigation Strategies

A. Geometric Redesigning

Ceramic thickness is crucial in mitigating electric field stress within (U)WBG power modules because the field intensity between electrodes is inversely proportional to their separation. Increasing the ceramic thickness, therefore, has a positive impact on electric field mitigation. F. Yan et al. [75] observed a 23% reduction in the initial 64.7 kV/mm electric field when they increased the AlN substrate thickness from 0.38 mm to 0.63 mm. Subsequently, the field dropped further to 28.6 kV/mm at a thickness of 2 mm, marking a 56% reduction. In another study [76], even though an 80% field reduction was achieved by increasing the AlN thickness from 0.63 to 1 mm, the benefit of increasing ceramic thickness was shown to diminish with further increments. While a 46% PDIV increase was observed from 0.38 mm to 0.63 mm, the increase was only 12% from 0.63 mm to 1 mm [77]. This suggests a slower rate of PDIV improvement with increasing thickness. Increasing ceramic thickness comes at the cost of compromised thermal performance as the thermal resistance between the die and baseplate rises, and additionally, thicker substrates add to the overall cost. This phenomenon is evident because the thermal conductivity of ceramic substrates is lower than that of metal electrodes. Considering all these factors collectively, pushing the ceramic thickness beyond 2 mm for HV modules (rated 25 kV or higher) to improve PDIV and reduce field stress is not recommended.

The length of one electrode within the power module can be adjusted while keeping the other constant to investigate the impact of a metal layer offset on electric field reduction. For instance, the offset of metallization layers for the geometry depicted in Fig. 7(a) is $r_{off}=r_u-r_i$. Here, r_u represents the distance between the substrate edge and the upper metal electrode, and r_i represents the distance to the lower metal electrode.

Fig. 7(b) illustrates the electric field values at four TPs for a metal offset layer ranging from -2 to 2 mm. As depicted in the plot, an increase in r_u and, consequently, r_{off} leads to an increase

in the electric field at P2, while it decreases at P3. This observation can be elucidated by noting that as the metal offset increases, the TP at P2 shifts in the right direction, experiencing greater compression from the bottom metal potential, and conversely, decreasing the metal layer offset by reducing r_u results in the opposite effect. Furthermore, it has been observed that altering r_{off} beyond these specified values gives rise to thermal management issues [75].

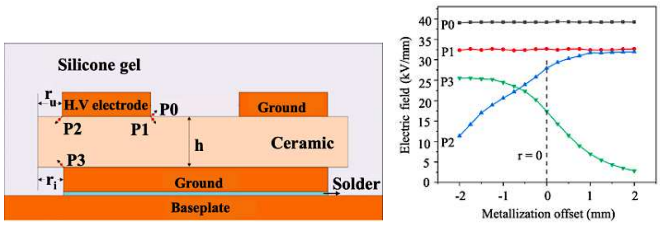

Fig. 7. (a) A diagram showing metal layer offset between two electrodes. (b) Plot of electric field at triple points with change in metal offset [75].

The idea of protruding the metal electrode on top of the substrate was introduced in [78] to prevent the formation of a TP at the metal edge, where the electric field tends to be the highest. This method proved to be highly effective in reducing the electric field at TP, thus allowing the use of a thin ceramic substrate to maintain good thermal performance. However, investigation in [79-81] into the efficacy of employing a protruding substrate to reduce the maximum field stress at TP revealed that the maximum field intensity on the SG and ceramic substrate at TP were 67.71 and 30.32 kV/mm respectively [79]. Despite showing a considerably higher reduction in field stress at ceramic substrate than SG, the electric field at SG and ceramic substrate still exceeded the specified criterion values of 17.48 kV/mm and 15.98 kV/mm. Hence, it is evident that the design of the protruding substrate is insufficient to achieve the desired dielectric performance.

The research in [79] introduces an innovative design that utilizes a stacked ceramic substrate design with a protruding substrate, which uses two substrates that collectively match the thickness of a standard case, in contrast to the conventional approach that employs a single substrate. The maximum electric field observed at both the AlN substrate and SG is impressively within the specified criterion values (15.18 and 17.48 kV/mm, respectively). However, these studies highlight the need for a thorough exploration of thermomechanical stability because ensuring the cohesion of substrates with bond lines featuring minimal structural defects and low interfacial thermal resistance demands a process of utmost reliability. This point is supported in [82], where the maximum temperature within the power module increased by 52% despite the electric field reduction and PDIV enhancement.

The investigation by H. Hourdequin et al. [83] revealed that incorporating a trench with a height of 0.6 mm and width of 0.5 mm on a 1 mm thick AlN substrate, resulted in a remarkable 57% reduction in the maximum field intensity at TP compared to the conventional structure. Furthermore, the study demonstrated a notable enhancement in PDIV from 7.2 kV to 9.2 kV when employing a 10 pC PD threshold. Still, the optimized electric field of 65 kV/mm is significantly higher than the breakdown strength of commercial SGs.

In [75], F. Yan et al. proposed an innovative ceramic substrate design, shown in Fig. 8(a), to isolate the weak insulation region corresponding to the interface of the ceramic substrate and encapsulant from TP, the area of high electric field concentration. Their findings indicated substantial field reductions of 26.56% and 48.85% at the metal edge and the substrate-gel interface, respectively, illustrated in Fig. 8(b). It was concluded that a notable decrease in electric field enhancement could be achieved by increasing the SG's height and diminishing the substrate's height beneath the upper metallization layer. Before integrating these methods into the insulation packaging of (U)WBG modules, it is imperative to conduct thorough thermal and mechanical stress evaluations, considering the alterations they induce in the geometric structure of the substrate.

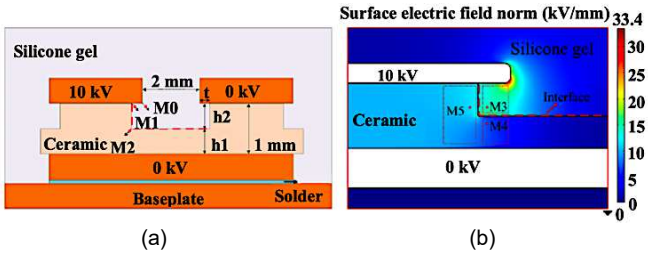

Fig. 8.(a) Innovative substrate design. (b) Electric field distribution [75].

B. Alternative Encapsulation Materials in Place of Silicone Gel

Research has found that the encapsulants used to safeguard the components of (U)WBG power modules from external factors like dust and humidity are a limiting factor in the high-temperature packaging of the modules compared to other components. This highlights the need to prioritize the long-term stability of encapsulants to ensure reliable packaging [73], [84]. Currently, SG and epoxy resin (EP) are the most commonly used encapsulants for packaging (U)WBG power modules. However, as the research on power modules advances to achieve higher limits of temperature and frequency, exploring alternative encapsulation materials that comply with the operating conditions becomes necessary.

Fig. 9 delineates the crucial attributes that polymeric encapsulation materials must embody to be suitable for high-voltage and high-power-density U(WBG) power modules [18]. A paramount consideration is the need for an encapsulation material with high TC and thermal diffusivity to ensure reliable performance at temperatures exceeding 250°C. Simultaneously, a high T_g becomes imperative, as it enables the encapsulant to maintain its structural integrity and mechanical properties within the demanding operating conditions. For seamless functionality under high frequencies, slew rates, and electric fields, several other fundamental properties including high volume resistivity, low relative permittivity (ε_r), and high dielectric strength are needed. Furthermore, from a manufacturing standpoint, low viscosity is desirable to facilitate the easy flow of materials within modules, minimizing the occurrence of defects. A low CTE is sought to prevent CTE

mismatches with other components that might induce thermomechanical stresses [33]. Additionally, low moisture absorption of the encapsulant is crucial to ensure the (U)WBG power modules perform optimally even under harsh weather conditions.

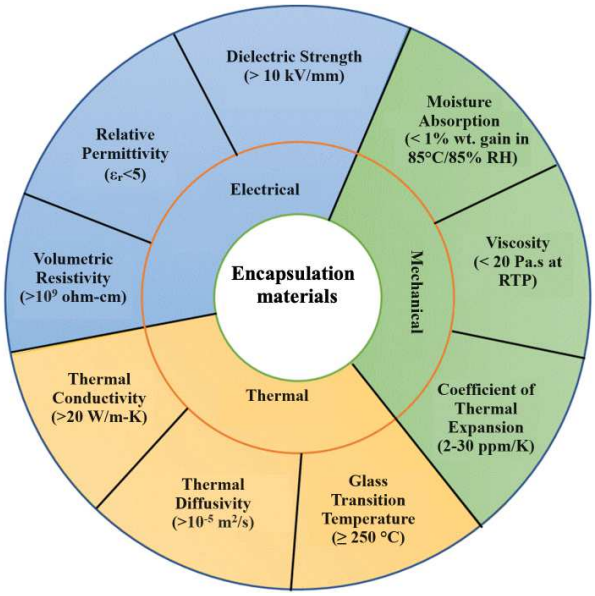

Fig. 9. Desired properties of high voltage, high power density encapsulation materials for HV applications [18] [33].

However, the current encapsulants, specifically SG and EP, fall short of achieving certain desired properties. Practical data reveals that SG exhibits a TC and CTE of 0.17 W/(m·K) and 1000 ppm/K, respectively. On the other hand, EP demonstrates a TC of 1 W/(m·K) and a T_g of 135°C, as documented in [44]. This underscores the ongoing challenge of aligning encapsulant properties with the exacting requirements of advanced (U)WBG power modules.

The study [85] examines the characteristics, potential, and constraints of encapsulation materials designed for high-temperature power modules. Among these materials, fluoric phthalonitrile resin, benzo-polymers, bio-based epoxy systems, and notably, the epoxy resin-cyanate ester (EP-CE) blend system incorporating Al_2O_3 fillers complemented by polyimide (PI) demonstrate promise owing to their notable attributes such as high T_g, reduced CTE, and enhanced TC. However, a comprehensive exploration is still required to thoroughly assess their processability, compatibility with other electronic materials, and dielectric properties.

The most common technique to enhance the thermal, mechanical, and electrical properties of the existing encapsulants is to include high thermal conductivity fillers [86]. These fillers, which could be micro or nano-sized, such as ZnO, SiC, and AlN, have been proven to not only increase the TC, reduce the CTE, and increase the T_g of the polymer matrix but also improve its dielectric characteristics. When these fillers are added to the polymer matrix, they form a network of conductive pathways that help to distribute the electric field more evenly throughout the material. This reduces the concentration of electric field at the triple points - the areas where the filler particles meet the polymer matrix - and prevents electrical breakdown. When these fillers are added to the EP and SG, they form a network of strong interfacial interactions with the epoxy and silicone matrix, which restricts the mobility of the polymer chains and reduces the free volume within the material [87]. This results in a more ordered and compact polymer structure, which increases the T_g of the epoxy resin and reduces the CTE of silicone gel. In particular, AlN and Al_2O3 have high TC, which helps to dissipate heat generated during the curing process [88]. This property is especially important for EPs, as excessive heat can cause degradation and reduce the T_g of the material. Moreover, the micro and nano-fillers also have a lower CTE than the silicone matrix, which helps to offset the overall CTE of the composite material. They act as a thermal bridge, transferring heat more efficiently throughout the material and reducing thermal gradients that can cause deformation.

B. X. Du et al. [89] studied the effect of adding micro-sized SiC fillers to the silicone rubber (SiR) matrix and found that the higher the filler content, the more significant the increase in the nonlinearity coefficient of the SiC/SiR composite and the reduction in electric field stress. However, this comes at the expense of a decrease in the insulation's breakdown strength, as the breakdown strength of the composite decreased from 17 kV/mm to 1.1 kV/mm with the addition of 50 parts per hundred (phr) filler. In a similar experiment, Q. Wang et al. [90] found that when micro SiC fillers are incorporated in elastomers, the maximum field intensity is lowered, and thermal performance is improved. However, the composite's tensile strength is reduced due to the appearance of defects on the large-sized microparticles-matrix interface, and the nonlinear conductivity characteristic is lost at high temperatures because the conductive paths are damaged due to aggressive movement of molecular chains [91]. Therefore, incorporating nanofillers into the polymer matrix is the best way to reduce the electric field stress at TP without compromising the breakdown strength, mechanical stability, and thermal performance.

In the study [92], adding as little as 10% of micro-sized and nano-sized SiC/AlN fillers to the SE matrix significantly enhanced its thermal properties. This inclusion elevates TC by 19%, lowers CTE by 11%, and boosts PDIV by 33% compared to the original pure SE encapsulant. However, the study did not explore the impact of nanofillers on the dielectric breakdown strength, nonlinearity characteristics, and mechanical stability, which are key factors that require further investigation. According to research conducted by X. Chen et al. [93], the optimal electrical properties of nano-AlN/micro-SiC/SE hybrid composite can be achieved by the inclusion of 3 wt% of AlN nanofiller. The enhanced electrical properties of the composite were examined through various experimental and simulation techniques such as nonlinear conductivity measurement, dielectric spectroscopy, DC breakdown strength test, thermally stimulated depolarization current (TSDC) experiment, and FEM electric field simulation. The study results indicate that the electric field stress at TP is reduced by 77% when a 10 kV voltage is applied, as depicted in Fig. 10(a). Moreover, the maximum electric field stress within the module increases slowly with increasing applied voltage, reaching only 13.77 kV/mm, enabling (U)WBG power modules to operate up to 32 kV, as illustrated in Fig. 10(b). The improvement in

electrical properties of SiR composites is closely linked to the cross-linking between the nanofillers and polymer matrix [94]. Cross-linking restricts the free movement of electrons, thereby reducing the free volume and the mean free path, and as a result, the energy electrons accumulate for breakdown is also reduced.

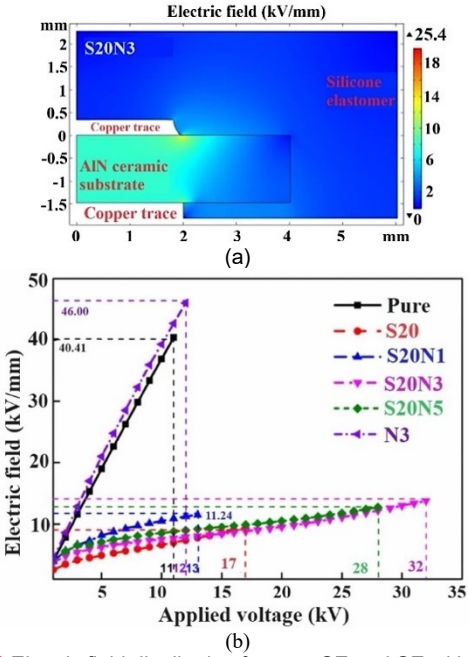

Fig. 10. (a) Electric field distribution for pure SE and SE with 3 wt% AlN fillers. (b) Plot of electric field with increase in applied voltage [93].

In [95], the hardness, tensile strength, and breaking elongation rate were assessed to evaluate the impact of zirconia nanoparticles (nano-ZrO_2) on the mechanical properties of SiR composites and the study revealed a 21% and 13% increment in the tensile strength and hardness, respectively, with negligible changes in the breaking elongation rate. This enhancement in mechanical stability was attributed to the increase in cross-linking degree with nanofiller content, which maintained structural integrity by forming a filler-polymer interface. However, the results obtained for cable accessories in [95] are contradictory to the findings of the investigation carried out for power modules in [90]. The study showed a 40% decrement in the tensile strength when 3 wt% AlN nanoparticles and 20 wt% of SiC microparticles were added to the SE matrix. This discrepancy could be attributed to the introduction of cracks and defects with large-sized fillers, as described in [96]. Therefore, further investigations are recommended to optimize all three (electrical, thermal, and mechanical) performances of composite silicone encapsulants with different filler contents and configurations.

X. Chen et al. [97] discovered that increasing the content of AlN nanofillers in EP used in (U)WBG power module encapsulation led to an increase in TC. However, T_g and breakdown strength initially increased by 11% and 25%, respectively, before decreasing, which suggests that a higher nanofiller content can cause agglomeration, forming voids and defects that reduce breakdown strength and T_g, evident in Fig. 11(a) and 11(b). A study with SiC nanoparticle incorporation on EP polymer matrix [98] supported this finding, as T_g increased to 136.8°C from 122.3°C with 2 wt% SiC addition, EP1, but decreased to 127.5°C with 5 wt% SiC, EP2, even though the nonlinear electrical and thermal conductivity was rising in all cases. The breakdown strength of EP1 was the highest, but it fell with adding more fillers, which the increase in space charge density and electric field distortion can explain. In [99], it was discovered that despite reducing the electric field stress at TP by 58% compared to pure EP matrix, the nonlinear conductivity characteristics of EP mixed with micro SiC particles degrade with temperature. This effect is due to the particle agglomeration hindering the optimal performance of highly conductive filler materials, consistent with the results obtained for nanofiller inclusion on SE polymers. Additionally, high micro filler loading can create many defects and voids in the filler-matrix interface, leading to insulation issues like a decrease in dielectric strength and an increase in dielectric loss. Therefore, combining microparticles with moderate inclusion of nanofillers has proved to be the best way to enhance an insulation system's thermal and dielectric performance [100].

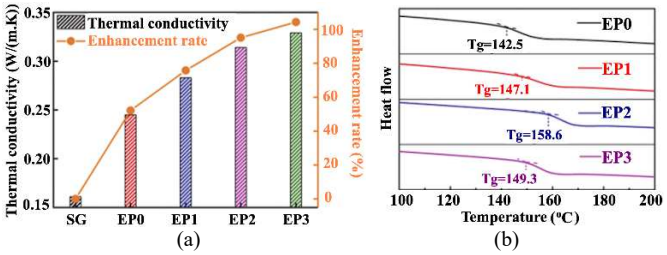

Fig. 11. (a) Enhancement in TC for EP with nanofillers inclusion. (b) T_g for pure EP and EP with different wt% of nanofillers [97].

Q. Wang et al. [101] studied the power loss within the power modules along with thermal and electrical characteristics to assess the effectiveness of using micro/nano hybrid nanoparticles in EP polymer matrix. The results showed the power loss to be the highest for 40 wt% micro-AlN and 5 wt% nano-AlN, and this effect was more severe at higher frequencies and temperatures. The addition of nano-AlN fillers can decrease the real permittivity of the EP, whereas the addition of micro-AlN fillers increases the imaginary permittivity, causing more dielectric loss. Therefore, the filler ratio and size should be carefully considered for hybrid composites as encapsulants. The ratio of the micro and nano fillers becomes particularly important for hybrid composite encapsulants because the use of an encapsulant in (U)WBG power modules involves a balance between electrical, thermal, and mechanical properties, and the change in the ratio between micro and nano-sized fillers creates dominance of one over the other. This is validated in [102] where the composite mixture of nano boron nitride (BN) with micro AlN fillers in EP matrix showed an increase in TC from 0.153 W/(m·K) to 1.449 (m·K) while T_g got reduced from 126.72°C to 105.46°C. A similar result was concluded in [103], where T_g decreased with the increase in nanofiller content as well as the size of the nanofillers. Y. Zhang et al. [104] used a BN/EP composite for high-frequency electric tree evaluation and found that adding BN sheets raised the tree inception voltage across all frequencies, exceeding 7 kV at 130 kHz compared to the 5.7 kV of pure EP. At 400 Hz and 130 kHz, the observed maximum and minimum tree lengths were 51.2% and 18.0% less than pure EP, as illustrated in Fig. 12(a) and 12(b).

Contrary to expectations, the 15% increase in TC with 0.1 wt% BN sheet didn't hinder the initiation and growth of electrical trees. Instead, the blockage caused by the BN sheet and the presence of deeper traps at the BN/EP interface, as presented in Fig. 12(c), played a pivotal role.

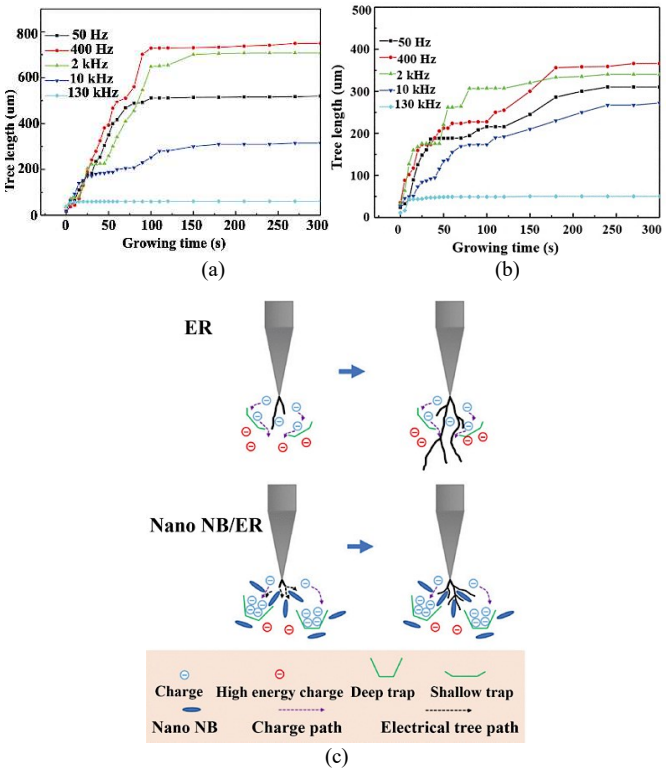

Fig. 12. (a) Tree lengths for pure EP. (b) Tree lengths for BN/EP composite. (c) Charge trapping phenomena with BN sheet [104].

This is further validated in [105], where the introduction of deep traps by KH560-dopamine (KD) in aramid fiber/epoxy resin (AP-EP) composites increased the breakdown strength by 39% due to the introduction of deeper traps that inhibit the migration of charge carriers. It has been suggested that higher nanofiller loading blocks the propagation path of electrical trees by introducing deep traps and reducing PD activity [106]. In [107], it was shown that the breakdown voltage of the EP/Al_2O_3 nanocomposites increased with increasing content of nanofillers and that the use of nanofillers can increase the TC of the composites. An electrical treeing analysis in [108] proposed the effectiveness of nanocomposites on electric trees mitigation to increase with a rise in temperature and rise in nanofiller content, as the phase resolved partial discharge (PRPD) pattern showed an absence of electrical trees at 140°C for 10-wt% silica nanofiller addition. The results seem promising, but the paper fails to study the effect of nanofiller addition on TC, T_g, breakdown strength, and most importantly, dielectric losses.

It is not often that papers explore the changes brought in the mechanical properties of EP composites when added with nanoparticles or microparticles. This is significant because the mechanical characteristics (especially fracture toughness) of an EP are a critical factor [109], limiting its use as an encapsulant in high voltage and high-power density applications of (U)WBG power modules. So, it is essential to investigate whether fillers that enhance the thermal and electrical properties of the composite have a positive impact on its mechanical stability. In a study by Y. Gong [110], it was observed that despite improving the TC of the composite, the addition of 40 wt% hexagonal boron nitride (h-BN) fillers reduced the tensile strength and breakdown strength compared to the pure EP by 32% and 53%, respectively. The decline in tensile and breakdown strength continued as the filler content increased, indicating the formation of defects and voids on the filler-polymer interface.

Among nonpolymeric materials, glass holds the most promise for use as an encapsulant in (U)WBG power modules because of its thermal stability for temperatures exceeding 250°C. Moreover, glass has good mechanical strength, thermal stability, and dielectric characteristics. However, limited research is available for its use as an encapsulation material, mainly because of its high processing temperature (>450°C) and cracking due to CTE mismatches with substrate that cause thermo-mechanical stresses. Glass encapsulants also suffer from high dielectric constant (8-12), high elastic modulus (58 GPa), and high viscosity (50+ Pa.s), which are the three critical parameters in terms of electric field stress and thermo-mechanical stability. One way to mitigate this would be to use a PI buffer layer between the glass encapsulant and ceramic substrate to minimize thermo-mechanical stresses due to high Young's modulus and CTE mismatches. The PDIV of glass with PI buffer was reduced by only 0.5 kV at 250°C than at 25°C, proving its high-temperature stability. However, the PDIV of glass-encapsulated DBC substrate with PI buffer was found to be reduced to 3.6 kV from 5.13 kV [111]. The reason for this was believed to be the formation of cracks or pores between glass and substrate instead of the high processing temperature of glass. This was further strengthened in [112], where multiple pores of diameter <1 mm were seen at the polyimide/substrate interface despite the uncoated DBC substrate being neat. This might help explain the 16.67% reduction in the average breakdown field strength of the encapsulant.

Therefore, even though PI buffer helps reduce the thermomechanical stresses induced by high Young's modulus of glass, it might be detrimental from a PD perspective. In [113], The optimal electrical insulation and the thermal properties of glass as a packaging material for SiC modules were obtained for 5 wt% BaO filler addition in glass. The T_g, which is 343.1°C, CTE, which is 11.48, and PDIV, which is around 7.5 kV, are better than currently used encapsulants. Still, the problem of high processing temperature (475°C for 35 minutes) and high dielectric constant (>24) are still persistent, suggesting the research should be focused on this area if the glass is to be used as a packaging material for (U)WBG power modules.

Polyimides (PIs) have garnered significant attention due to their exceptional material characteristics, including superb thermal resistance and stability, high resistance to chemicals, outstanding corrosion resistance, impressive mechanical properties, and excellent adhesive capabilities. Despite their remarkable qualities, there is a pressing need for enhancements in the mechanical and thermal aspects, along with

improvements in the hydrophobic properties of PIs. These advancements are essential to effectively address the rapidly growing and increasingly stringent requirements in power module packaging.

Table IV: Properties of Polyimide (PI) encapsulant with various additives

Materials	T_g (°C)	$T_{5\%}$ (°C)	Tensile strength (MPa)	Ref.
PI	298.3	513.4	98	[114]
PI/Si_3N_4 (2%)	343.5	549.7	152	
PI/Si_3N_4(10%)	348.0	567.5	202	
PI	259	454.6	/	[116]
PI/Si_3N_4 (3%)	279	519.4		
PI/Si_3N_4 (7%)	279	538.8		
PI-1	390	412	97.9±2.1	[117]
PI-4	294	405	94.5±2.0	
PAI-10-0	441	493	77	[118]
PAI-7-8	401	459	118	
LC-PI_I	332.8	/	105	[120]
LC-PI_{IV}	327.2		119	
CF_3- BPTP/ PDA: 5/95	378	592	192	[119]
CF_3- BPTP/ PDA: 30/70	314	471	103	
BPTP/PDA: 5/95	393	580	194	
BPTP/PDA: 30/70	331	550	178	

The enhanced properties of PIs with various additives are summarized in Table IV. Mekuria et.al. [114] achieved 106%, 16.7%, and 9.5% improvement in Tensile strength, T_g, and $T_{5\%}$ with 10 wt% Si_3N_4 filler incorporation into a pure PI matrix. This is attributed to the decrease in moisture content from 1.9 to 0.625% due to hydrophobic properties of Si_3N_4 particles. Both the thermal and mechanical properties of Si_3N_4/PI composite were improving with higher filler loadings, which is contradicted by the findings in [115]. The tensile and breakdown strengths of PI/3% TN composite were 18.5% and 24.8% lower than PI/ 0.25% TN composite. This can be explained as follows: the significant enhancement in mechanical performance with the incorporation of a small amount of TNs (0.25 wt%) into the PI matrix is primarily attributed to the robust interactions established between TNs and the PI matrix. However, when the TNs doping content surpasses a specific threshold (approximately 0.25 wt% in this investigation), the proximity between TNs decreases, leading to a more random alignment of TNs orientation. Consequently, this results in the formation of relatively thinner layers of the PI matrix, causing a reduction in both the tensile strength and elongation at break of the PI/TNs composite films. Nevertheless, a compelling body of evidence from [116], [117], [118], and [119], consistently highlights the superior tensile strength, T_g, and $T_{5\%}$ values exhibited by both PI and PI composites in comparison to currently utilized encapsulants. Moreover, noteworthy characteristics such as TC exceeding 2 W/m-K [120] and breakdown strength surpassing 200 kV/mm further underscore PI's potential for integration into (U)WBG power modules. Despite these promising attributes, the imperative next step involves the practical incorporation of these composites into existing power modules to validate their viability for real-world applications.

From the research conducted so far, it is evident that the alternatives to currently used encapsulant materials possess better thermal, electrical, and mechanical properties than the conventional ones. However, the desired characteristics outlined in the chart have yet to be achieved, as the TC is still low, and the increase in T_g and reduction in CTE of EP and SG are still below the desired percentages. Furthermore, most studies have yet to consider mechanical stress's effect while assessing alternative encapsulants' efficiency, which may limit their performance below optimal capability. The research on new encapsulation materials like glass and PI is still recent as their practical implementation on power modules has been rarely done. It is important to note that the composite matrix's properties depend on various factors, including the complex network, cross-linking degree, filler size, filler content, and the baseline properties of the encapsulant and filler itself. Therefore, it is impossible to make a general case on how adding fillers to conventional encapsulation materials improves their properties. This highlights the need for more attention to a holistic review of alternative encapsulants, considering all three characteristics - electrical, thermal, and mechanical - for their possible use in high voltage, high power density (U)WBG power modules.

C. Nonlinear Field-Dependent Permittivity (FDP) Materials

It has been suggested that the permittivity of the encapsulant can be controlled in such a way that the imbalance in electric properties in the substrate-encapsulant interface reduces, forming a uniform electric field and reducing the electric field stress at TP [121]. The nonlinear field-dependent permittivity (FDP) materials take advantage of a high nonlinear dielectric constant feature of ferroelectric materials (e.g., $BaTiO_3$), which are incorporated as fillers into polymers (e.g., EP) having excellent processability and high breakdown strength [122]. The combination of these features in the polymer-filler composite helps in electric field reduction, PDIV improvement, and breakdown strength enhancement, as the ε_r of these functionally graded materials (FGM) used as encapsulants will increase with the increase in electric field stress.

The relationship between electric field and relative permittivity for 15% $BaTiO_3$ filled SG was given in [123] as $\varepsilon_r = 6.4 + 1.3E$. The mechanism behind the behavior of nonlinear FDP materials is based on the idea of increased permittivity in insulation materials where high stress occurs within a non-uniform field. This leads to a change in the distribution of the electrical field and a decrease in maximum stress at TPs [124]. When an electric field is applied to a material, the electric dipoles within the material tend to align themselves with the direction of the electric field. This alignment leads to an increase in the polarization of the material, which in turn leads to an increase in the dielectric constant of the material [125]. In these materials, the degree of alignment of the electric dipoles or the crystalline domain alignment of the material is field-dependent, which means that the degree of polarization and the dielectric constant of the material increase as the electric field strength increases. This field-dependent behavior is because the electric dipoles within the material experience a greater torque as the electric field strength increases, which leads to a greater degree of alignment. As a result of this behavior, the nonlinear FDPs with their nonlinear permittivity according to electric stress distributions

can absorb a significant amount of the electric field energy, which reduces the magnitude of the electric field at the triple points. This reduction in electric field strength helps to mitigate the occurrence of PD phenomenon.

Even though the utilization of nonlinear FDP materials in (U)WBG power modules looks promising, only limited research is being done in this area due to the disappearance of the nonlinear FDP properties of these materials above a specific temperature, curie point [123]. Previous studies have shown that this temperature is usually in the range of 125°C-145°C, considerably lower than the operating temperature of envisaged (U)WBG power modules.

U. Waltrich et al. conducted one of the first experimental investigations on a high permittivity composite material used as a TP coating, as reported in [126]. The metallic and Al_2O_3 ceramic edges were coated with EP, possessing a dielectric constant of 9, and encapsulated on all sides with SG, with a dielectric constant of 2.7. The findings showcased a noteworthy 10% reduction in the electric field due to the coating, and the substrate coated with a 40 wt% EP exhibited a PDIV of 13.6 kV, marking a substantial 43% enhancement compared to the uncoated substrate. However, at an 80 wt% EP coating, this value dropped to 12 kV, highlighting the influence of the high viscosity of the high ε_r ferroelectric material. In a similar investigation where $BaTiO_3$ particles are mixed with the EP matrix, the dielectric constant with 40 vol% $BaTiO_3$/EP composite increased to 16 from 2.7. However, the study also suggested that the dielectric loss increased with an increase in filler content due to nanoparticle agglomeration [127]. A study by A. Escriva et al. [128] examined the breakdown strength of $BaTiO_3$/EP nanocomposites and concluded a positive correlation between breakdown field reduction and filler thickness for fillers thicker than 100 μm, even though the thickness dependency for fillers up to 100 μm was deemed insignificant. The results also showed that the effect of filler content on breakdown field reduction gradually decreased, with lower effects observed between 20 vol% and 30 vol% filler loading compared to that between 1 vol% and 5 vol%. This can be explained by the fact that the higher the ferroelectric particle concentration, the higher the chance for more percolation conductive paths, leading to potential damage to the sample.

According to an investigation conducted by L. Zhong et al. [129], it was found that adding 33 vol% $BaTiO_3$ resulted in a 15% reduction of E_{max} compared to pure EP, due to an increase in ε_r to 11.7. However, the experiment also revealed that the viscosity of the material rose to more than 8000 mPa·s (millipascal second), which can cause complications during the material flow in power modules. This may lead to manufacturing defects, such as unfilled voids and cavities, and consequently, the insulation performance of the encapsulation materials may be compromised. In [130], F. Yan et al. proposed a valuable analysis that sheds light on the curie temperature of ferroelectric materials not reducing when encapsulated by polymeric encapsulants. The experiment indicates a significant reduction in the electric field at TP and inhibitions in tree-length propagation due to the presence of the $BaTiO_3$-gel interface. However, the study also suggests that fully coating the encapsulant area by composite might be detrimental to the (U)WBG power modules' performance, as it leads to an increment in dielectric loss and a reduction in dielectric breakdown strength with filler inclusion and an increase in temperature. Therefore, two strategies can be adopted to improve the insulation systems of these envisioned power modules. The first strategy is to apply functionally graded partial coating to the protrusions and TP, and the second strategy is to use ferroelectric materials with higher curie temperature, as the analysis indicated that the reduction in curie temperature when ferroelectric materials are encapsulated is negligible.

In [131], it was observed that despite the dielectric constant of $SrTiO_3$ being almost 7 times lower than $BaTiO_3$, the dielectric constant of the EP/$SrTiO_3$ composite was higher, and dielectric losses were lower than the EP/$BaTiO_3$ composite. Additionally, the TC of both nanocomposites was higher than that of the pure EP matrix. Specifically, the TC of the EP/$SrTiO_3$ composite was 29% and 40% higher than the EP/$BaTiO_3$ composite for 10 and 20 wt% loading, respectively. Furthermore, the study found that the space charge accumulation around the HV electrode was higher for $BaTiO_3$, suggesting inferior interfacial characteristics and the presence of more defects and voids than the $SrTiO_3$ nanocomposite. This highlights that having a higher ε_r of the ferroelectric material does not necessarily lead to a higher ε_r of the composite and, consequently, superior properties. The maximum electric field of the EP/$SrTiO_3$ composite was also found to be lower than that of EP/$BaTiO_3$ in [132], where the electrophoresis process was applied under AC voltage, which resulted in anisotropic composites. The anisotropic composites had higher ε_r than isotropic composites due to the alignment of particles with the changing direction of the applied voltage. However, increasing the filler content led to a significant reduction in the breakdown voltage of the composite due to the enhanced ionic or electronic transport along the chain direction.

Experimental investigations and FEM simulations have provided significant insights into the effects of areas far from TP and protrusions towards electric field reduction and PDIV enhancement showing these areas have a significantly lesser impact on the factors mentioned above. This has led to the development of field grading materials (FGM), which can address this issue. Nonlinear FDP coating or nonlinear capacitive FGM can be achieved with electrophoresis, which functionally grades the coating based on the electric field, increasing the permittivity of the composite material in areas of high electric field, and gradually decreasing it when moving away from them. This makes it possible to considerably reduce TP's electric field and mitigate issues related to PD and electrical trees. H. Yao et al. [29] used this principle to examine the effect in field reduction when replacing FGM material covering 51% of the encapsulation region with material covering only the micro-region (Fig. 13(a)) and discovered a negligible increase in electric field (from 18.51 to 18.86 kV/mm), further strengthening the theory that it is the area closest to TP that affects field reduction. One of the major advantages of this approach is the reduction in dielectric loss, as seen in Fig. 13(b).

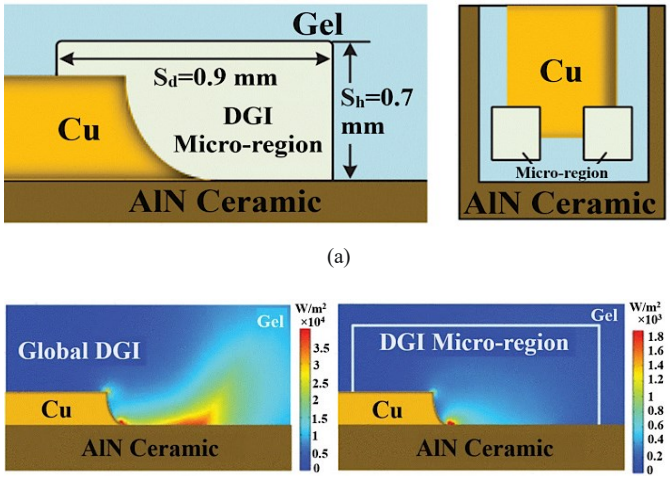

Fig. 13. (a) Front and top view of FGM micro-region. (b) Dielectric loss density distribution for 51% coating and micro coating, respectively [29].

In a series of three articles, S Diaham et al. delved into the principles of electrophoresis, its application in both uniform and non-uniform fields, and the analysis of electric field reduction and PDIV improvement through the use of nonlinear FDP nanocomposites produced via this process [133], [134], [135]. The use of $SrTiO_3$ as the ferroelectric material of choice in these experiments due to its high breakdown strength and, perhaps most notably, its negative curie temperature ensures that the material will not interfere with the performance of (U)WBG power modules at elevated temperatures, making it an ideal choice for these types of applications. The EP/$SrTiO_3$ nanocomposite is made thicker and has higher filler content in the FGM layer where the electric field stress is high, and thinner with lower filler content in the FGM bulk areas where the electric field stress is lower [133]. The thickness and filler content of the nanocomposite depends on the electrophoretic field and the duration of the electrophoresis process. However, inhomogeneity in the permittivity values in different regions around the HV electrode is possible, just like the inhomogeneity observed between low permittivity encapsulant and high permittivity substrate. A sudden change in the dielectric values between layers can lead to a buildup of space charges at the interface, reducing the dielectric breakdown strength. To mitigate this issue, it is recommended to maintain a lower electrophoretic field while increasing the duration of the electrophoresis process to increase the thickness of the FGM layer around the HV electrode. The permittivity is increased by 450% in the FGM layer region but only 55% in the bulk region, reducing the abrupt change in permittivity across the insulating materials. When applying electrophoresis under a non-uniform field created by sharp metallic edges and TPs in a power module, it was seen that the fillers arrange themselves in such a way that the concentration of filler is increased towards areas of high electric field created by TP and gradually decrease moving away from TP, depicted in Fig. 14(a). This, in turn, increases the permittivity of the region with higher filler loading, and a gradual decrease of permittivity can be seen while moving away from the TP, shown in Fig. 14(b) [134]. To observe the effectiveness of FGMs in electric field reduction and PDIV improvement, electric field simulations were performed on pure epoxy, homogeneous epoxy/$SrTiO_3$ composite, and FGM composites. The results showed that for the optimal permittivity range ($15 \leq \varepsilon_{layer} \leq 50$) of the FGM layer, the field reduction exceeded 50%, and the breakdown voltage improved by 68% compared to pure EP [135]. These findings, illustrated in Fig. 14(c), hold great promise; however, complementary investigations are necessary to observe the increase in viscosity of FGM composites, as the viscosity of high permittivity materials poses the most significant challenge in achieving advanced insulation systems.

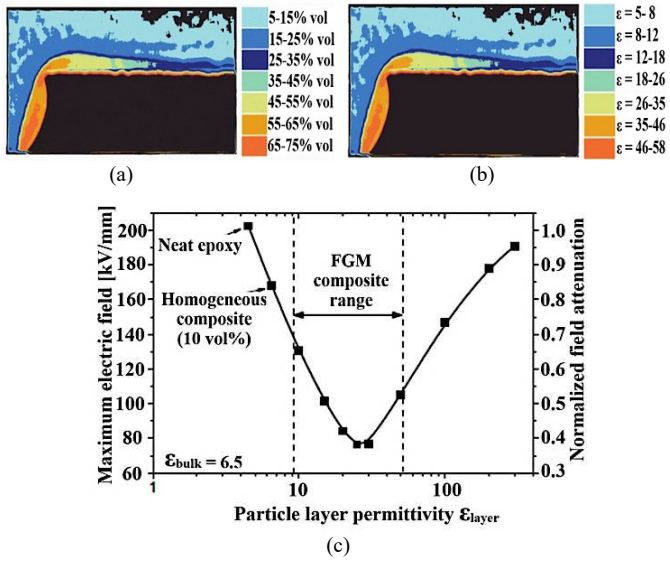

Fig. 14. (a) Grading of filler materials. (b) High permittivity in high electric field areas. (c) Plot of electric field with FGM layer permittivity [134], [135].

D. Nonlinear Field-Dependent Conductivity (FDC) layers

Nonlinear FDC composites are materials that involve the combination of conductive or semiconductive filler particles, such as zinc oxide micro varistors, with a polymer matrix like silicon rubber or epoxy resin [136], [137]. Space charges accumulate within the insulation materials due to low mobility of free charges in their structure. As a result, the electric field stress becomes higher in those areas of space charge accumulation, leading to nonuniform electric field distribution, significantly restricted to TPs and their surroundings. Nonlinear conductivity based on electric field is a phenomenon where the conductivity of a material changes in response to an applied electric field [138]. The mechanism behind this is based on the impact ionization effect, which occurs when high-energy electrons collide with the atoms in the material, generating additional electron-hole pairs. The newly generated carriers can contribute to the conductivity of the material, leading to an increase in conductivity with increasing electric field strength. In nonlinear FDC materials, this is a nonlinear process, which means that the increase in conductivity is not proportional to the increase in electric field strength. Instead, the increase in

conductivity becomes more pronounced as the electric field strength increases [139].

The use of nonlinear conductivity based on electric field can help mitigate the electric field stress in several ways. Firstly, the increased conductivity of the material reduces the electric field strength at the TPs, which helps to mitigate the occurrence of PD phenomenon. This is because the electric charges are less likely to accumulate at TPs, which reduces the likelihood of PD occurrence. Secondly, the increased conductivity of the material can also help reduce the electric field stress at other points in the device. This is because the increased conductivity leads to a more uniform distribution of the electric field, which helps to reduce the magnitude of the electric field stress throughout the device. The relationship between the electric field stress and the nonlinear conductivity of FDC materials is given as $\sigma(E) = \sigma_0(1 + (E/E_b)^{\alpha-1})$.

The composites' electric field grading mechanism is based on two crucial aspects: switching field (E_b) and nonlinearity coefficient (α). In these composites, once the electric field becomes higher than the specific value, the electrical conductivity of the composites increases by several orders of magnitude. The filler particles' percolation level, size, and shape can be adjusted to manipulate both parameters. To display nonlinear properties, the filler concentration level must surpass a threshold value known as the percolation threshold, which differs for different composites depending on the original polymeric matrix [140]. For instance, the percolation threshold for the ZnO-silicone rubber composite and the ZnO-epoxy composite is 35% and 20%, respectively. When the concentration level is below the percolation threshold, the composite behaves like an insulator because conduction paths cannot be established; meanwhile, a higher concentration level results in more conduction paths in the composite due to the shortening of the filler distance, leading to lower E_b. Also, studies have shown that to perform a frequency-independent operation, α should be greater than 10, and E_b should equal the applied voltage divided by the FDC layer length [141].

Extensive research has been conducted over the years on nonlinear FDC materials to address the challenges of high electric field and PD, and tremendous progress has been made towards finding solutions to these problems. In a study by K. Li et al. [142], the PRPD pattern shows less frequency and lower magnitude of PD pulses in addition to the inhibition of tree growth when nonlinear FDC coating comprised of SiC fillers on SG is applied to TP region (Fig. 15). They hypothesized that the positive impact of FDC coating introduction on electric field reduction strengthens with the increase in temperature owing to the apparent increase in conductivity of SG with temperature, leading to a reduction in electric field distortion. They attributed the 33% improvement in PDIV with a 73% reduction in electric field intensity to the principle that a 3-4 kV/mm reduction in electric field yields a 1 kV improvement in PDIV [143]. Therefore, the properties of FDC composites depend upon different parameters such as the permittivity/conductivity of the polymer matrix, the permittivity/conductivity of the filler particle and its size, and its content [144, 145].

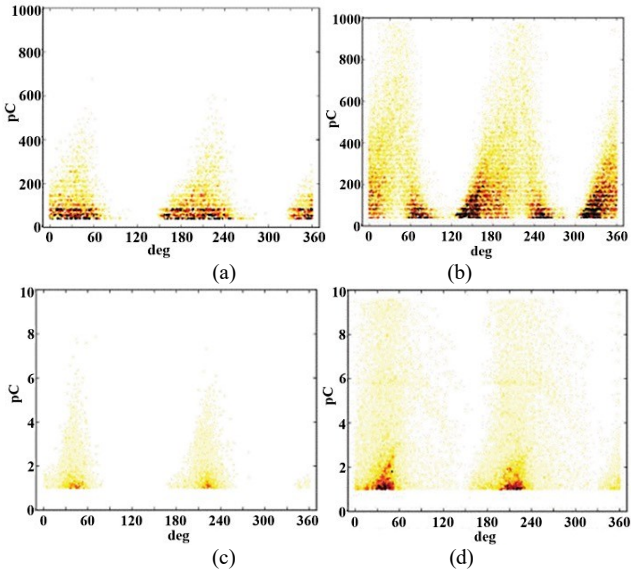

Fig. 15. PRPD patterns for: (a) 8 kV without nonlinear FDC coating. (b) 12 kV without coating. (c) 8 kV with coating. (d) 12 kV with coating [142].

J. Li et al. [146] observed an increment of 42% in PDIV when the SG encapsulant in 15 kV SiC power device is replaced with 60 wt% SiC filled FDC layer. Even though the viscosity of the FDC layer wasn't an issue due to its value being only 1350 mPa·s, the PDIV kept on decreasing with the increase in the thermal cycle, reducing by nearly 70% and reaching 3 kV after 1000 cycles. The decrease in PDIV is related to the weakening of the cross-linking degree between the filler and the polymer matrix and the formation of cracks and voids on the SG surface. Thus, despite having 50% higher PDIV compared to SG after 1000 thermal cycles, the degradation of FDC characteristics limits its application in (U)WBG power modules to lower temperatures and life cycles. In a similar experiment [147], the nonlinear FDC layer comprised of SiC/EP composite applied to HV electrode trenches was examined where the PDIV of the composite decreases with an increase in the number of thermal cycles during the thermal shock test, despite enhancing PDIV by 86% and minimizing electric field by 33% initially. The reduction is considerably lower for SiC/EP composite compared to SiC/SG composite because the thermal degradation in the latter case is due to the diminution of the cross-lining degree between nonlinear conductive filler and SG, which forms cracks and voids susceptible to the initiation of PD and electrical treeing activities. However, the mechanical stress is higher on EPs as validated by its high Young's modulus of elasticity, leading to the desire to reduce its Young's modulus for thermos-mechanical stability [148], [149]. Understanding nonlinear FDC layers' thermal and mechanical traits is essential in assessing their suitability for high-temperature, high-voltage power modules. A study [150] investigated a polyimide-based FDC (PI-FDC) layer infused with SiC nanofillers, and the findings revealed that a composition of 50 phr PI-FDC with 500 nm SiC particles exhibited heightened values of E_b and α, along with reduced field intensity and increased PDIV. Notably, this coating maintained its nonlinear conductivity even after 120 hours at 200°C, a significant contrast to FDC coatings on EP and SG matrices that only lasted 24 hours.

Thermal analysis further corroborated these results as no 5% weight loss was observed until reaching 537.5°C. Additionally, the layer's lower Young's modulus mitigated thermal stress during thermal shock tests, showcasing its reliability in terms of thermo-mechanical performance.

J. Xu et al. [151] delved into the realm of nonlinear resistive coatings or FDC layers, intending to determine their optimal properties for shielding TP in MV power modules, which is presented in Table V. Upon applying an FDC coating to reduce the electric field at TP, a new TP is formed at the junction of the coating, encapsulant, and substrate, shown in Fig. 16. Having a high value of E_b results in the nonlinear FDC coating achieving the field-dependent conductivity property after a higher value of the electric field, which might result in the electric field at the encapsulant (which has lower dielectric strength) exceeding its dielectric strength and resulting in PD. Therefore, a lower value of E_b might seem favorable as the FDC coating's field-dependent high conductivity will incept even at a lower electric field, thus effectively reducing the electric field at the junction of the metal electrode, polymer encapsulant, and ceramic substrate. However, this has proved to increase the electric field at the newly formed TP because of the significant difference in conductivity between the substrate-coating and encapsulant-coating interfaces [152]. Therefore, to reduce the electric field at the TP and not increase the electric field at the newly formed TP beyond the criterion limit, a balance must be maintained on all the parameters that the characteristics of the FDC layer depend on.

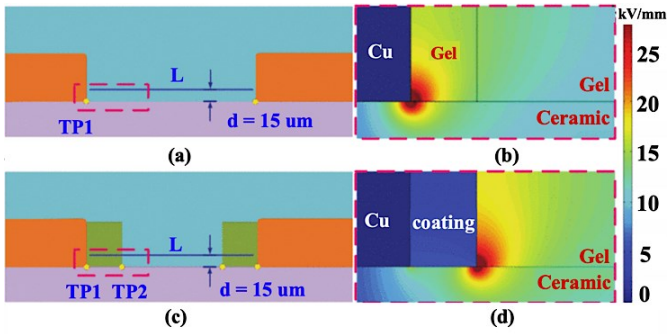

Fig. 16. (a) conventional structure and (b) Electric field distribution. (c) nonlinear FDC coating and (d) Electric field distribution [151].

Table V: Desired optimal properties of nonlinear FDC layers [151].

Switching field value, E_b (kV/mm)	Applied Voltage (U_{peak})/ Trench Distance (d)
Nonlinearity coefficient (α)	10
Relative permittivity (ε_r)	5
Low-field conductivity, σ_0 (S/m)	1.4×10^{-9}
Coating coverage at each sharp edge of electrode (m)	5-25%

A rectangular or a triangular coating to cover TP changes its location and introduces a new triple junction [76] and even though the electric field at this newly formed junction is lower compared to the TP of conventional structure, an imbalance in either σ_0, E_b, ε_r or α might lead to undesirably high electric field and initiate PD activity. The value of electrical conductivity, contact resistance, E_b, and ε_r is also shown to be dependent on the filler shape, size, and content [153]. For example, a high value of the nonlinearity coefficient helps the FDC layer achieve higher conductivity in a shorter time frame, leading to a better influence on electric field reduction at TP, but it also decreases electrode spacing, hindering thermal performance. Therefore, [154-157] introduced a new design of nonlinear resistive field grading coating, in which the triple junction is formed at the end line of the ceramic substrate where the effect of a high electric field is negligible due to the distance from TP. In [158], a nonlinear FDC coating was developed at the TP of the upper metal electrode, and it was discovered that while the field stress around SG and AlN substrate remained within acceptable limits, it increased around the ground electrode. This was because, for $E>E_b$, the field stress around the HV electrode was transferred to the ground electrode due to the FDC coating. To address this issue, they proposed a protruding substrate design with a bridging nonlinear FDC layer, resulting in the field stress being within criterion values (17 kV/mm and 25 kV/mm for SG and substrate, respectively). Moreover, the study [79] underscored that a protruding substrate design for both metallization layers, in conjunction with a comprehensive bridging nonlinear FDC coating covering the substrate-to-baseplate area, yielded maximal field reduction. Although promising, the combined effect of an FDC layer with high permittivity (ε_r=12) and a modified substrate design warrants further investigation to understand the alteration in substrate behavior under these conditions comprehensively.

It has been discovered that coating nonlinear FDC or FDP materials could alleviate high electric field stress and PD issues at TP but fail to reduce PD activity in voids or air cavities due to high electric field stress within them. Therefore, a new approach of implementing an electret layer, a dielectric material with an electric charge or dipole orientation, has been proposed to resolve the PD issues [159], [160], [161]. This approach has shown promising results, as evidenced by Fig. 17, which demonstrates a reduction in the electric field within bubbles and cavities within laminated busbars when an electret layer is introduced, along with electric field reduction at other critical points [161].

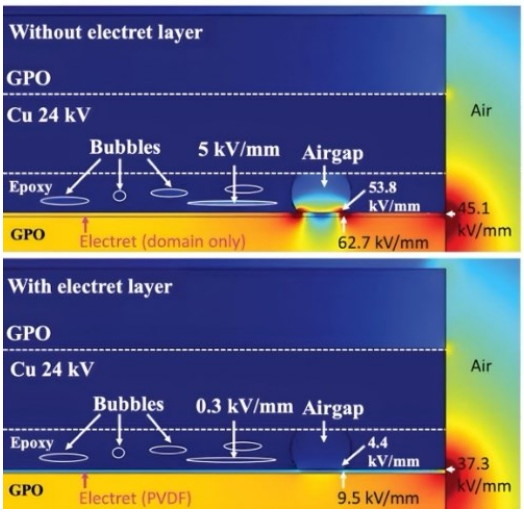

Fig. 17. Electric field distribution showing the mitigation of electric field stress within airgap by implementing electret layer [161].

Table VI: A comparative analysis of electric field stress reduction and PDIV improvement with various mitigation strategies

Mitigation strategy	Ref.	Encapsulant	Ceramic substrate	Mitigation method	Emax before (kV/mm)	Emax after (kV/mm)	Average PDIV before (kV)	Average PDIV after (kV)
Geometric redesigning	[75]	SG	AlN	Ceramic thickness- 0.63 mm	64.7 (for 0.38 mm)	49.82	/	/
				Ceramic thickness- 2 mm		28.5		
	[76]	SG	AlN	Ceramic thickness- 1 mm	45 (for 0.63 mm)	9	/	/
	[77]	/	Al2O3	Ceramic thickness=0.63 mm	36 (for 0.38 mm)	29	8	11.5
			AlN	Ceramic thickness=1 mm	29 (for 0.63 mm)	24	12	13.5
	[83]	SG	AlN	mesa structure	154	65	7.2	9.2
	[78]	SG	AlN	Protruding substrate	42.06	22.53	4.7	3.48
FDC layers	[142]	SG	AlN	10 wt% SiC-filled epoxy resin	23.2	8.3	7.80	10.40
	[146]	SG	AlN	60 wt% SiC-filled silicone gel	/	/	6.9	9.8
				stacked DBC+ SiC-filled SG	57.42	18.35		18.31
	[147]	SG	/	Pure epoxy resin coating	32	30.5	6.5	7.2
				29.2 vol% SiC-filled epoxy resin		20.3		12.1
				34.0 vol% SiC-filled epoxy resin		21.1		12.15
	[150]	SG	Al_2O_3	5 um PI coated SiC/EP FDC	31.018	20.85	7.3	/
				2 um PI coated SiC/EP FDC		19.32		/
				500 nm PI coated SiC/EP FDC		18.72		11.3
	[151]	SG	Al_2O_3	10% coated ZnO-filled SG	25.4	17.9	/	/
					24.1	14.4		
FDP materials	[123]	SG	AlN	15 vol% BaTiO3-filled SG (fixed ε)	44	39.8	9	/
				15% BaTiO3-filled SG (nonlinear ε)		31.1		12.2
	[129]	EP	AlN	33.2 vol% BaTiO3-filled EP	40.1	34.2	/	/
				40 vol% BaTiO3-filled EP		53.6		
	[130]	SG	AlN	15 vol% BaTiO3-filled SG at 500 Hz	/	/	19.63 (BV)	18.68 (BV)
				15 vol% BaTiO3-filled SG at 10 kHz			18.77 (BV)	17.80 (BV)
	[131]	EP	/	15 wt% BaTiO3-filled EP	/	/	11.41	12.5
				15 wt% SiTiO3-filled EP				13.17
				40 wt% BaTiO3-filled EP				13.51
				40 wt% SiTiO3-filled EP				13.77
	[132]	EP	/	10 wt% BaTiO3-filled EP	~115	~49	/	/
				10 wt% SrTiO3-filled EP		~41		
Alternative encapsulant	[90]	SE	AlN	20 wt% m-SiC-filled SE	36.9	7.4	/	/
				3 wt% AlN & 20 wt% SiC-filled SE		6.6		
	[92]	SE	/	5 vol% n-BN and m-SiC-filled SE	/	/	3	3.8
				10 vol% n-BN and m-SiC-filled SE				4.1
				40 vol% n-BN and m-SiC-filled SE				4.5
	[93]	SE	AlN	3 wt% AlN & 20 wt% SiC-filled SE	36.9	7.4	11 (MAV)	32 (MAV)
				5 wt% AlN & 20 wt% SiC-filled SE		8.5		28 (MAV)
				3 wt% AlN-filled SE		39.3		12 (MAV)
	[98]	EP	AlN	1 wt% SiCw-filled EP	/	3.52	~103.5 kV/mm (DBS)	~124.5 kV/mm
				3 wt% SiCw-filled EP		13.1		~20.5 kV/mm
				5 wt% SiCw-filled EP		26.3		~12 kV/mm
	[97]	SG	AlN	Pure EP	60.5	58.5	53.8 kV/mm (ABS)	49.2 (ABS)
				2 wt% n-AlN-filled EP		57.5		61.6 (ABS)
				3 wt% AlN-filled EP		57		53.5 (ABS)
	[107]	EP	/	10 wt% m-Al2O3-filled EP	/	/	19.9	21.2
				40 wt% m-Al2O3-filled EP				18.5

BV= Breakdown voltage, MAV= Maximum acceptable voltage, DBS= DC breakdown strength, ABS= AC breakdown strength

This study has shown that introducing an electret layer can reduce the electric field at TP from 118.4 kV/mm to 59 kV/mm, a 50% reduction while mitigating the electric field stress within air cavities, voids, and bubbles. However, the electret layer has low Tc, which could jeopardize the heat dissipation efficiency of the substrate. So, further investigation is required to observe the effect of Tc when high Tc fillers like SiC particles are added to the electret and the electret thickness layer is minimized.

VI. Challenges, Opportunities, And Future Scope

B. Challenges

1) The challenge with the next-generation encapsulation materials isn't just about achieving one specific property, but rather a combination of several properties that are essential for the high temperature, high power density, and high-frequency operation of (U)WBG power modules, such as TC, mechanical strength, CTE, T_g, and viscosity.

2) The issue with ceramic substrate materials is that although their properties are superior to encapsulation materials and significant progress has been made in finding alternative substrates with better properties, practical research in WBG power modules is still limited to Al_2O_3 and AlN as substrates. While Al_2O_3 suffers from poor thermal conductivity, AlN with better properties than Al_2O_3 also has lower tensile and fracture strength.

3) Despite being proposed as an alternative encapsulation material, the challenge with the currently available options is that they are still based on SG and EP as a base matrix for the composites. As the properties of original matrix are very low, the improvement seen with these micro- and nanocomposites is very limited. This results in a significant limitation in the improvement of thermal, mechanical, and electrical characteristics that are desired.

4) One notable issue is that harsh weather conditions are not always considered when investigating electric field and PD analysis. This can lead to a severe impact on the performance of insulating materials, further degrading their properties. Harsh operation conditions, such as low pressure for aircraft, moisture exposure in ships, and high thermal and radiation aging, can have a significant influence on the stability of these materials over time.

5) Even though mitigation strategies have provided promising solutions, they are not based on real-world conditions where (U)WBG power modules will work, such as high dv/dt square waveform, high frequency, and temperatures exceeding 250°C. High frequency causes space charge accumulation leading to electric field distortion, increase in tree lengths, and change in electrical tree morphology from branch type to dense bush-like structures with the presence of voids and bubbles, which have lower dielectric characteristics than the insulation materials (encapsulant and substrate). The high frequency also impacts the self-healing properties of SG, as the PD cavity propagates before its discharge track can disappear.

6) It is also worth noting that the IEC standard, IEC 61287-1, which was made for sinusoidal AC conditions, may not apply to the operational conditions of (U)WBG power modules.

B. Opportunities and future scope

1) Si3N4 can be a viable ceramic substrate material for (U)WBG power modules. However, there are two main issues with Si_3N_4: lower thermal conductivity and higher cost. While significant progress has been made in increasing the thermal conductivity of Si_3N_4 substrate materials beyond 150, making them cost-effective remains a challenge. Nevertheless, from the perspective of next-generation (U)WBG power modules, where researchers and engineers are continuously trying to reduce the size, Si_3N_4's higher thermal stability, even with lower thickness, seems to be a promising solution.

2) While research in WBG materials like SiC and GaN has made significant progress, it is reaching saturation. Therefore, the focus should shift to (U)WBG materials like diamond and Ga_2O_3. Research should focus on improving these materials' properties, such as increasing the TC of Ga_2O_3 and improving the processability and cost-effectiveness of diamond.

3) Alternative encapsulants like PI and glass should be given priority. While their properties have been validated to be superior to traditional encapsulants, there is still a need for more PD and electric field stress analysis in power module packaging applications to verify their compatibility with metallization layers and encapsulants.

4) Epoxy nanocomposites have shown considerable superiority in reducing electric field distortion and PD issues due to the formation of matrix/filler interface. They improve the barrier height needed to be surpassed for space charge injection, and their shallow traps avoid space charge accumulation. Additionally, their TC is improved due to the formation of a thermally conductive path. They have displayed that these PD inhibition properties are not only for low frequencies (50 or 500 Hz) but also for higher frequencies (18 kHz). However, these values are still lower than the frequency under which (U)WBG power modules will be operating. Thus, future research must investigate space charge, electrical treeing, and PD activities in nanocomposites under higher frequencies (>100 kHz).

5) The array of functionally graded materials (FGMs), such as FDP materials and FDC layers, should be expanded. Currently, FGMs based on EP and SG matrix are only studied, but more investigations on SE and Cyanate Ester (CE), which have better properties than SG and EP, need to be carried out.

6) Further research on electrets is needed as they can address the issue of voids within encapsulants. However, their PDIV analysis is still not mature enough, and they display a loss in TC, which is crucial for heat dissipation. Additionally, their mitigation effect on actual operating conditions of temperatures more than 100 °C and higher frequency has not been conducted.

7) Research should be conducted at operating conditions as close to practical operating conditions of (U)WBG power modules as possible, which means temperatures greater than 200°C, frequencies greater than 100 kHz, and a square wave voltage waveform.

8) Finally, the current IEC standard, IEC 61287-1, under which PD analysis is validated is for power frequency AC voltages and may not work for high-frequency square pulses. Therefore, a change in the IEC standard is needed to reflect the practical operating conditions of (U)WBG modules.

VII. Conclusion

This paper reviews the recent advancements to tackle the challenge of high electric field stress and partial discharge within insulation systems for envisaged high voltage, high-power-density U(WBG) power modules in detail. It explores the critical role of the TP in reducing field stress and scrutinizes the weaknesses of current encapsulation materials (SG and EP) in terms of space charge characteristics, PD, and electrical treeing activity. The effect of harsh weather conditions on the insulation properties of these materials are discussed in detail. With the anticipated exposure of (U)WBG power modules to elevated operating temperatures, the study evaluates the thermal stability of potential alternative materials to replace SG and EP. Additionally, the paper examines research on redesigned substrate structures (mesa structure, protruding substrate, and stacked substrate), non-linear field-dependent permittivity (FDP) materials, and non-linear field-dependent conductivity (FDC) coatings to achieve decreased electric field and enhanced PDIV levels. However, it underscores that most investigations have been conducted below 200°C, significantly lower than the envisioned 500°C operational range, primarily under DC and power frequency sinusoidal AC voltages. Notably, PD behavior under fast-rise high-frequency square wave voltages differs from power frequency sinusoidal voltages. Consequently, existing standards fall short in predicting the insulation performance of power electronics modules under real-world conditions involving high temperatures, rapid voltage slew rates, and repetitive voltage pulses. Furthermore, the existing standard of PD detection in power modules, IEC 61287-1, primarily standardized for AC sinusoidal voltages, fails to give a precise estimation for these situations. This underscores the need for a new standard to assess module insulation performance accurately. Hence, future research must concentrate on accurate estimation of PD pulses with proper standards, investigation of insulation systems under high slew rate square pulses with high frequencies, and operation of power modules under elevated temperatures to thoroughly evaluate the effectiveness of mitigation methods.

VI. References

[1] "How We're Moving to Net-Zero by 2050," Energy.gov. Accessed: Dec. 28, 2023. [Online]. Available: https://www.energy.gov/articles/how-were-moving-net-zero-2050

[2] A. Barzkar and M. Ghassemi, "Components of electrical power systems in more and all-electric aircraft: A review," *IEEE Trans. Transp. Electrification*, vol. 8, no. 4, pp. 4037–4053, Dec. 2022.

[3] Y. Chen, A. Iradukunda, H. A. Mantooth, Z. Chen, and D. Huitink, "A tutorial on high-density power module packaging," *IEEE J. Emerg. Sel. Top. Power Electron.*, vol. 11, no. 3, pp. 2469–2486, Jun. 2023.

[4] N. Keshmiri, D. Wang, B. Agrawal, R. Hou, and A. Emadi, "Current status and future trends of GaN HEMTs in electrified transportation," *IEEE Access*, vol. 8, pp. 70553–70571, 2020.

[5] P. E, P. K. B, C. B, E. Manikandan, and L. Agarwal, "A comprehensive review of recent progress, prospect and challenges of silicon carbide and its applications," *Silicon*, vol. 14, no. 18, pp. 12887–12900, Dec. 2022.

[6] Y. Yang, L. Dorn-Gomba, R. Rodriguez, C. Mak, and A. Emadi, "Automotive power module packaging: Current status and future trends," *IEEE Access*, vol. 8, pp. 160126–160144, 2020.

[7] S. M. S. H. Rafin, R. Ahmed, M. A. Haque, M. K. Hossain, M. A. Haque, and O. A. Mohammed, "Power electronics revolutionized: A comprehensive analysis of emerging wide and ultrawide bandgap devices," *Micromachines*, vol. 14, no. 11, Art. no. 11, Nov. 2023.

[8] H. Jain, S. Rajawat, and P. Agrawal, "Comparision of wide band gap semiconductors for power electronics applications," in *proc. Int. Conf. Recent Adv. Microw. Theory Appl., 2008, pp. 878-881.*

[9] M. Borghei and M. Ghassemi, "Separation and classification of corona discharges under low pressures based on deep learning method," *IEEE Trans. Dielectr. Electr. Insul.*, vol. 29, no. 1, pp. 319–326, Feb. 2022.

[10] M. Borghei and M. Ghassemi, "Insulation materials and systems for more- and all-electric aircraft: A review identifying challenges and future research needs," *IEEE Trans. Transport. Electrific.*, vol. 7, no. 3, pp. 1930–1953, Sept. 2021.

[11] M. Ghassemi, "Accelerated insulation aging due to fast, repetitive voltages: A review identifying challenges and future research needs," *IEEE Trans. Dielectr. Electr. Insul.*, vol. 26, no. 5, pp. 1558–1568, Oct. 2019.

[12] D. Kenfaui *et al.*, "Innovative ceramic-matrix composite substrates with tunable electrical conductivity for high-power applications," *Sci. Technol. Adv. Mater.*, vol. 23, no. 1, pp. 735–751, Dec. 2022.

[13] L. Wang, Z. Zeng, P. Sun, S. Ai, J. Zhang, and Y. Wang, "Electric-Field-Dominated partial discharge in medium voltage SiC power module packaging: Model, mechanism, reshaping, and assessment," *IEEE Trans. Power Electron.*, vol. 37, no. 5, pp. 5422–5432, May 2022.

[14] B. Zhang, M. Ghassemi, and Y. Zhang, "Insulation Materials and Systems for Power Electronics Modules: A review identifying challenges and future research needs," *IEEE Trans. Dielectr. Electr. Insul.*, vol. 28, no. 1, pp. 290–302, Feb. 2021.

[15] Z. Huang, C. Chen, Y. Kang, S. Munk-Nielsen, and C. Uhrenfeldt, "Mitigation measures of the electric field in the medium-voltage power module: Effect of voltage types and recommendations for designers," *High Volt.*, vol. 6, no. 5, pp. 836–849, 2021.

[16] H. Lee, V. Smet, and R. Tummala, "A review of SiC power module packaging technologies: Challenges, advances, and emerging issues," *IEEE J. Emerg. Sel. Top. Power Electron.*, vol. 8, no. 1, pp. 239–255, Mar. 2020.

[17] G. Moreno, S. Narumanchi, X. Feng, P. Anschel, S. Myers, and P. Keller, "Electric-Drive vehicle power electronics thermal management: Current status, challenges, and future directions," *J. Electron. Packag.*, vol. 144, no. 011004, Aug. 2021.

[18] M. Lokanathan, P. V. Acharya, A. Ouroua, S. M. Strank, R. E. Hebner, and V. Bahadur, "Review of nanocomposite dielectric materials with high thermal conductivity," *Proc. IEEE*, vol. 109, no. 8, pp. 1364–1397, Aug. 2021.

[19] M. Ghassemi, "PD measurements, failure analysis, and control in high-power IGBT modules," *High Volt.*, vol. 3, no. 3, pp. 170–178, 2018.

[20] M. Ghassemi, "Electrical insulation weaknesses in wide bandgap devices," in *Simulation and Modelling of Electrical Insulation Weaknesses in Electrical Equipment*, IntechOpen, 2018.

[21] J. Deltour, M.-L. Locatelli, S. Dinculescu, D. Malec, and D. Meyer, "Partial discharges and AC breakdown voltage tests on thick metallized aluminum nitride substrates for high voltage power modules," in *Proc. IEEE Electr. Insul. Conf. (EIC)*, 2023, pp. 1–5.

[22] I. Semenov, I. F. Gunheim, K. Niayesh, H. K. H. Meyer, and L. Lundgaard, "Investigation of partial discharges in AlN substrates under fast transient voltages," *IEEE Trans. Dielectr. Electr. Insul.*, vol. 29, no. 2, pp. 745–752, Apr. 2022.

[23] Z. Yang, K. Li, X. Jiang, B. Zhang, and X. Li, "The degradation behaviors from triple junctions in IGBT power modules," in *Proc. IEEE Int. Conf. High Voltage Eng. and Appl. (ICHVE)*, 2022, pp. 1–5.

[24] A. M. Aliyu and A. Castellazzi, "Prognostic system for power modules in converter systems using structure function," *IEEE Trans. Power Electron.*, vol. 33, no. 1, pp. 595–605, Jan. 2018.

[25] Y. Wang, Y. Ding, and Y. Yin, "Reliability of wide band gap power electronic semiconductor and packaging: A review," *Energies*, vol. 15, no. 18, Art. no. 18, Jan. 2022.

[26] M. M. Tousi and M. Ghassemi, "Effects of frequency and temperature on electric field mitigation method via protruding substrate combined with applying nonlinear FDC layer in wide bandgap power modules," *Energies*, vol. 13, p. 2022, 2020.

[27] H. You, Z. Wei, B. Hu, R. Na, and J. Wang, "A comprehensive PD study method on power modules with ultra-high dv/dt output," in *Proc. IEEE 7th Workshop Wide Bandgap Power Devices Appl. (WiPDA)*, 2019, pp. 214–218.

[28] A. B. Jørgensen, S. Munk-Nielsen, and C. Uhrenfeldt, "Overview of digital design and finite-element analysis in modern power electronic packaging," *IEEE Trans. Power Electron.*, vol. 35, no. 10, pp. 10892–10905, Oct. 2020.

[29] H. Yao *et al.*, "Two-Stage electric field optimization method for high-voltage power module using dielectrically graded insulation micro-region," *IEEE Trans. Dielectr. Electr. Insul.*, vol. 30, no. 3, pp. 1005–1015, Jun. 2023.

[30] Z. Valdez-Nava, D. Kenfaui, M.-L. Locatelli, L. Laudebat, and S. Guillemet, "Ceramic substrates for high voltage power electronics: past, present and future," in *Proc. IEEE Int. Workshop Integr. Power Packag. (IWIPP)*, 2019, pp. 91–96.

[31] K. Hirao, Y. Zhou, and H. Miyazaki, "3 - Substrate," in *Wide Bandgap Power Semiconductor Packaging*, K. Suganuma, Ed., in Woodhead Publishing Series in Electronic and Optical Materials. Woodhead Publishing, 2018, pp. 81–94.

[32] W. Wang *et al.*, "ZrSi2–MgO as novel additives for high thermal conductivity of β-Si3N4 ceramics," *J. Am. Ceram. Soc.*, vol. 103, no. 3, pp. 2090–2100, 2020.

[33] Y. Qin *et al.*, "Thermal management and packaging of wide and ultra-wide bandgap power devices: a review and perspective," *J. Phys. Appl. Phys.*, vol. 56, no. 9, p. 093001, Feb. 2023.

[34] C. Chen, F. Luo, and Y. Kang, "A review of SiC power module packaging: Layout, material system and integration," *CPSS Trans. Power Electron. Appl.*, vol. 2, no. 3, pp. 170–186, Sep. 2017.

[35] X. Zhu, H. Hayashi, Y. Zhou, and K. Hirao, "Influence of additive composition on thermal and mechanical properties of ß–Si3N4 ceramics," *J. Mater. Res.*, vol. 19, no. 11, pp. 3270–3278, Nov. 2004.

[36] F. Hu, T. Zhu, Z. Xie, and J. Liu, "Effect of composite sintering additives containing non-oxide on mechanical, thermal and dielectric properties of silicon nitride ceramics substrate," *Ceram. Int.*, vol. 47, no. 10, Part A, pp. 13635–13643, May 2021.

[37] H. Miyazaki *et al.*, "Improved resistance to thermal fatigue of active metal brazing substrates for silicon carbide power modules using tough silicon nitrides with high thermal conductivity," *Ceram. Int.*, vol. 44, no. 8, pp. 8870–8876, Jun. 2018.

[38] Y. Nakashima *et al.*, "Effect of microstructures on dielectric breakdown strength of sintered reaction-bonded silicon nitride ceramics," *J. Am. Ceram. Soc.*, vol. 106, no. 2, pp. 1139–1148, 2023.

[39] Y. Zhou, H. Hyuga, D. Kusano, Y. Yoshizawa, T. Ohji, and K. Hirao, "Development of high-thermal-conductivity silicon nitride ceramics," *J. Asian Ceram. Soc.*, vol. 3, no. 3, pp. 221–229, Sep. 2015.

[40] F. Hu, Z.-P. Xie, J. Zhang, Z.-L. Hu, and D. An, "Promising high-thermal-conductivity substrate material for high-power electronic device: silicon nitride ceramics," *Rare Met.*, vol. 39, no. 5, pp. 463–478, May 2020.

[41] B. Zhang *et al.*, "Electrical properties of silicone gel for WBG-based power module packaging at high temperatures," *IEEE Trans. Dielectr. Electr. Insul.*, vol. 30, no. 2, pp. 852–861, Apr. 2023.

[42] L. M. Salvatierra *et al.*, "Self-healing during electrical treeing: A feature of the two-phase liquid-solid nature of silicone gels," *IEEE Trans. Dielectr. Electr. Insul.*, vol. 23, no. 2, pp. 757–767, Apr. 2016.

[43] B. Zhang *et al.*, "Dielectric properties characterization and evaluation of commercial silicone gels for high-voltage high-power power electronics module packaging," *IEEE Trans. Dielectr. Electr. Insul.*, vol. 30, no. 1, pp. 210–219, Feb. 2023.

[44] S. Kaessner, M. G. Scheibel, S. Behrendt, B. Boettge, C. Berthold, and K. G. Nickel, "Reliability of novel ceramic encapsulation materials for electronic packaging," *J. Microelectron. Electron. Packag.*, vol. 15, no. 3, pp. 132–139, Jul. 2018.

[45] Y.-J. Chen, H.-C. Chen, W.-H. Chi, H.-C. Hsu, K.-C. Lu, and H.-K. Liao, "Epoxy resin encapsulated IGBT module characteristics and reliability," in *Proc. Int. Microsystems, Packaging, Assembly Circuits Techno. Conf. (IMPACT)*, 2019, pp. 120–123.

[46] C. Dai, X. Chen, T. Jiang, A. Paramane, and Y. Tanaka, "Improvement of electrical and material properties of epoxy resin/ aluminum nitride nanocomposites for packaging materials," *Polym. Test.*, vol. 86, p. 106502, Jun. 2020.

[47] H. Zhang *et al.*, "Optimization of boron nitride sphere loading in epoxy: Enhanced thermal conductivity and excellent electrical insulation," *Polymers*, vol. 11, no. 8, Art. no. 8, Aug. 2019.

[48] X. Zhu, X. Guan, L. Dai, X. Cui, J. Fan, and Z. Fang, "Improvement of electrical insulating properties for defective metal/epoxy resin interface in power modules by micro-plasma jet," *Appl. Surf. Sci.*, vol. 638, p. 158064, Nov. 2023.

[49] K. Zhang, G. Schlottig, E. Mengotti, O. Quittard, and F. Iannuzzo, "Study of moisture transport in silicone gel for IGBT modules," *Microelectron. Reliab.*, vol. 114, p. 113773, Nov. 2020.

[50] K. Li, B. Zhang, Z. Yang, X. Jiang, and X. Li, "Degradation behaviors of silicone gel encapsulation material with moisture intrusion," *Polym. Degrad. Stab.*, vol. 206, p. 110197, Dec. 2022.

[51] B. Francis, "Water absorption studies in epoxy nanocomposites," in *Epoxy Composites*, John Wiley & Sons, Ltd, 2021, pp. 241–258.

[52] F. N. Alhabill, H. Bhabha, S. Harmer, A. S. Vaughan, Y. Wang, and D. Qiang, "On the dynamics of moisture absorption and its impact on dielectric properties of epoxy networks under DC and AC voltages," *IEEE Trans. Dielectr. Electr. Insul.*, vol. 28, no. 5, pp. 1677–1685, Oct. 2021.

[53] F. Zeng, D. Su, R. Chen, Q. Yao, L. Li, and J. Tang, "Effect of thermal oxidative aging on cross-linking network and electrical property of silicone gel for IGBT packaging," *IEEE Trans. Dielectr. Electr. Insul.*, pp. 1–1, 2023.

[54] N. Zavatta, F. Rondina, M. P. Falaschetti, and L. Donati, "Effect of thermal ageing on the mechanical strength of carbon fibre reinforced epoxy composites," *Polymers*, vol. 13, no. 12, Art. no. 12, Jan. 2021.

[55] H. Yao *et al.*, "Dielectric characteristic analysis and insulation state evaluation of packaging material for power module with different aging degrees," *IEEE Trans. Dielectr. Electr. Insul.*, vol. 31, no. 1, pp. 513–522, Feb. 2024.

[56] J. Wu, K. Niu, B. Su, and Y. Wang, "Effect of combined UV thermal and hydrolytic aging on micro-contact properties of silicone elastomer," *Polym. Degrad. Stab.*, vol. 151, pp. 126–135, May 2018.

[57] T. Kaneko, S. Ito, T. Minakawa, N. Hirai, and Y. Ohki, "Degradation mechanisms of silicone rubber under different aging conditions," *Polym. Degrad. Stab.*, vol. 168, p. 108936, Oct. 2019.

[58] M. Borghei and M. Ghassemi, "Effects of low-pressure condition on partial discharges in WBG power electronics modules," in *Proc. IEEE Electr. Insul. Conf. (EIC)*, 2020, pp. 199–202.

[59] M. Borghei and M. Ghassemi, "A finite element analysis model for partial discharges in silicone gel under a high slew rate, high-frequency square wave voltage in low-pressure conditions," *Energies*, vol. 13, no. 9, Art. no. 9, Jan. 2020.

[60] M. Awais *et al.*, "Investigating optimal region for thermal and electrical properties of epoxy nanocomposites under high frequencies and temperatures," *Nanotechnology*, vol. 33, no. 13, p. 135705, Jan. 2022

[61] Y. Wang *et al.*, "Space-Charge accumulation and its impact on high-voltage power module partial discharge under dc and PWM waves: testing and modeling," *IEEE Trans. Power Electron.*, vol. 36, no. 10, pp. 11097–11108, Oct. 2021.

[62] C. Dai, Y. Tanaka, H. Miyake, K. Sato, X. Chen, and A. Paramane, "Space charge dynamics in epoxy based composites under dc and square pulse wave of different polarities and frequencies," *IEEE Trans. Dielectr. Electr. Insul.*, vol. 28, no. 6, pp. 1980–1987, Dec. 2021.

[63] X. Chen, C. Dai, Z. Hong, M. Awais, A. Paramane, and Y. Tanaka, "Charge dynamics and thermal properties of epoxy based micro and nano hybrid composites at high temperatures," *J. Appl. Polym. Sci.*, vol. 138, no. 28, p. 50676, 2021.

[64] C. Dai, Y. Tanaka, H. Miyake, K. Sato, X. Chen, and A. Paramane, "Space-Charge characteristics in epoxy composites under square pulse wave of different polarities with various frequencies at various temperatures," *IEEE Trans. Dielectr. Electr. Insul.*, vol. 29, no. 1, pp. 137–144, Feb. 2022.

[65] S. Nakamura *et al.*, "Electrical treeing in silicone gel under repetitive voltage impulses," *IEEE Trans. Dielectr. Electr. Insul.*, vol. 26, no. 6, pp. 1919–1925, Dec. 2019.

[66] M. Borghei and M. Ghassemi, "Partial discharge analysis under high-frequency, fast-rise square wave voltages in silicone gel: A modeling approach," *Energies*, vol. 12, no. 23, Art. no. 23, Jan. 2019.

[67] M. Borghei and M. Ghassemi, "Investigation of low-pressure condition impact on partial discharge in micro-voids using finite-element analysis," in *Proc. IEEE Energy Convers. Congr. & Expo. (ECCE)*, 2020, pp. 3293–3298.

[68] M. Borghei and M. Ghassemi, "Characterization of partial discharge activities in WBG power converters under low-pressure condition," *Energies*, vol. 14, no. 17, Art. no. 17, Jan. 2021.

[69] H. You, Z. Wei, B. Hu, Z. Zhao, R. Na, and J. Wang, "Partial discharge behaviors in power modules under square pulses with ultrafast dv/dt," *IEEE Trans. Power Electron.*, vol. 36, no. 3, pp. 2611–2620, Mar. 2021.

[70] J. Wang, C. Chen, H. Yan, W. Wang, L. Zou, and L. Zhang, "Electrical trees of silicone gel encapsulation materials in power electronic modules self-healing properties and influencing factors," *IEEE Trans. Ind. Appl.*, vol. 60, no. 1, pp. 1288–1297, Jan. 2024.

[71] F. Yan, L. Wang, H. Wang, and C. Zhang, "Electrical trees in silicone gel influenced by different frequency and pulse width under unipolar high frequency square wave voltage," *IEEE Trans. Dielectr. Electr. Insul.*, pp. 1–1, 2024.

[72] Q. Wang, X. Chen, A. Paramane, J. Li, X. Huang, and N. Ren, "Design of interfacial electrical tree-resistant packaging insulation using grafted silicone elastomer nanocomposites for high-temperature power modules," *IEEE Trans. Power Electron.*, pp. 1–14, 2024.

[73] Y. Lin *et al.*, "Temperature- and degradation-dependent maximum electric field stress in wire-bonding power modules under PWM waves," *IEEE J. Emerg. Sel. Top. Power Electron.*, vol. 10, no. 6, pp. 7653–7664, Dec. 2022.

[74] Y. Ding, Y. Wang, H. Sun, and Y. Yin, "High-Temperature partial discharge characteristics of power module packaging insulation under square pulse with high dv/dt based on down-mixing method," *IEEE Trans. Ind. Electron.*, vol. 70, no. 7, pp. 7334–7342, Jul. 2023.

[75] F. Yan, L. Wang, Y. Gan, K. Li, and B. Zhang, "A new structure of ceramic substrate to reduce the critical electric field in high voltage power modules," *J. Electron. Packag.*, vol. 144, no. 031016, Mar. 2022.

[76] M. Ghessemi, "Geometrical techniques for electric field control in (ultra) wide bandgap power electronics modules," in *Proc. IEEE Electr. Insul. Conf. (EIC*), 2018, pp. 589–592.

[77] C. F. Bayer, U. Waltrich, R. Schneider, A. Soueidan, E. Baer, and A. Schletz, "Enhancing partial discharge inception voltage of DBCs by geometrical variations based on simulations of the electric field strength," *in Proc. IEEE Int. Conf. Integr. Power Electronics Systems (CIPS)*, 2016, pp. 1–5.

[78] H. Reynes, C. Buttay, and H. Morel, "Protruding ceramic substrates for high voltage packaging of wide bandgap semiconductors," in *Proc. IEEE 5th Workshop Wide Bandgap Power Devices Appl. (WiPDA),* 2017, pp. 404–410.

[79] M. M. Tousi and M. Ghassemi, "Combined geometrical techniques and applying nonlinear field dependent conductivity layers to address the high electric field stress issue in high voltage high-density wide bandgap power modules," *IEEE Trans. Dielectr. Electr. Insul.*, vol. 27, no. 1, pp. 305–313, Feb. 2020.

[80] M. M. Tousi and M. Ghassemi, "Electrical insulation packaging for a 20 kV high density wide bandgap power module," in *Proc. IEEE Energy Convers. Congr. & Expo. (ECCE)*, 2019, pp. 4162–4166.

[81] M. M. Tousi and M. Ghassemi, "Nonlinear resistive electric field grading in high-voltage, high-power wide bandgap power module packaging, " in *Proc. IEEE Energy Convers. Congr. & Expo. (ECCE)*, 2019, pp. 7124–7129.

[82] A. Deshpande, F. Luo, A. Iradukunda, D. Huitink, and L. Boteler, "Stacked DBC cavitied substrate for a 15-kV half-bridge power module," in *Proc. IEEE Int. Workshop Integr. Power Packag. (IWIPP)*, 2019, pp. 12–17.

[83] H. Hourdequin, L. Laudebat, M.-L. Locatelli, Z. Valdez-Nava, and P. Bidan, "Metallized ceramic substrate with mesa structure for voltage ramp-up of power modules," *Eur. Phys. J. Appl. Phys.*, vol. 87, no. 2, Art. no. 2, Aug. 2019.

[84] Y. Xiao, Z. Zhang, M. S. Duraij, T.-G. Zsurzsan, and M. A. E. Andersen, "Review of high-temperature power electronics converters," *IEEE Trans. Power Electron.*, vol. 37, no. 12, pp. 14831–14849, Dec. 2022.

[85] H. Gao and P. Liu, "High-Temperature encapsulation materials for power modules: technology and future development trends," *IEEE Trans. Compon. Packag. Manuf. Technol.*, vol. 12, no. 11, pp. 1867–1881, Nov. 2022.

[86] K. K. Khanum and S. H. Jayaram, "Improved thermal properties and erosion resistance of silicone composites with hexagonal boron nitride," *IEEE Trans. Ind. Appl.*, vol. 58, no. 5, pp. 6583–6590, Sep. 2022.

[87] R. Yadav, M. Singh, D. Shekhawat, S.-Y. Lee, and S.-J. Park, "The role of fillers to enhance the mechanical, thermal, and wear characteristics of polymer composite materials: A review," *Compos. Part Appl. Sci. Manuf.*, vol. 175, p. 107775, Dec. 2023.

[88] T. Li, P. Li, R. Sun, and S. Yu, "Polymer-based nanocomposites in semiconductor packaging," *IET Nanodielectrics*, vol. 6, no. 3, pp. 147–158, 2023.

[89] B. X. Du, Z. R. Yang, Z. L. Li, and J. Li, "Temperature-dependent nonlinear conductivity and carrier mobility of silicone rubber/SiC composites," *IEEE Trans. Dielectr. Electr. Insul.*, vol. 25, no. 3, pp. 1080–1087, Jun. 2018.

[90] Q. Wang, X. Chen, X. Huang, A. Muhammad, A. Paramane, and N. Ren, "Enhanced field-dependent conductivity and material properties of nano-AlN/micro-SiC/silicone elastomer hybrid composites for electric stress mitigation in high-voltage power modules," *Nanotechnology*, vol. 33, no. 47, p. 475706, Sep. 2022.

[91] Q. Wang, X. Chen, X. Huang, A. Paramane, and N. Ren, "Generating nonlinear conductive characteristics of micro-silicon carbide/silicone elastomer composites at high temperature utilizing nano-AlN fillers," *Mater. Lett.*, vol. 321, p. 132423, Aug. 2022.

[92] Y. Wang, J. Wu, Y. Yin, and T. Han, "Effect of micro and nano-size boron nitride and silicon carbide on thermal properties and partial discharge resistance of silicone elastomer composite," *IEEE Trans. Dielectr. Electr. Insul.*, vol. 27, no. 2, pp. 377–385, Apr. 2020.

[93] X. Chen, Q. Wang, X. Huang, A. Muhammad, A. Paramane, and N. Ren, "Enhancement of electrical properties by including nano-aluminum nitride to micro-silicon carbide/silicone elastomer composites for potential power module packaging applications," *J. Mater. Sci. Mater. Electron.*, vol. 33, no. 23, pp. 18768–18785, Aug. 2022.

[94] Y.-W. Fu, Y.-Q. Zhang, W.-F. Sun, and X. Wang, "Functionalization of silica nanoparticles to improve crosslinking degree, insulation performance and space charge characteristics of UV-initiated XLPE," *Molecules*, vol. 25, no. 17, Art. no. 17, Jan. 2020.

[95] X. Zhu, Y. Zhou, Y. Zhang, L. Zhou, and X. Huang, "The effects of nano-ZrO_2 on the mechanical and electrical properties of silicone rubber and a corresponding mechanism analysis," *IEEE Trans. Dielectr. Electr. Insul.*, vol. 29, no. 6, pp. 2218–2226, Dec. 2022.

[96] X. Zhao *et al.*, "Filler size effect on tuning electrical, mechanical, and thermal properties of field grading composites," *CSEE J. Power Energy Syst.*, vol. 9, no. 2, pp. 743–750, Mar. 2023.

[97] X. Chen, Q. Wang, N. Ren, C. Dai, M. Awais, and A. Paramane, "Potential of epoxy nanocomposites for packaging materials of high voltage power modules: A validation using experiments and simulation," *IEEE Trans. Dielectr. Electr. Insul.*, vol. 28, no. 6, pp. 2161–2169, Dec. 2021.

[98] X. Chen, Q. Wang, X. Huang, M. Awais, A. Paramane, and N. Ren, "Investigation of electrical and thermal properties of epoxy resin/silicon carbide whisker composites for electronic packaging materials," *IEEE Trans. Compon. Packag. Manuf. Technol.*, vol. 12, no. 7, pp. 1109–1121, Jul. 2022.

[99] R. Li, Y. Wang, C. Zhang, H. Liang, J. Li, and B. Du, "Non-Linear conductivity epoxy/SiC composites for emerging power module packaging: fabrication, characterization and application," *Materials*, vol. 13, no. 15, Art. no. 15, Jan. 2020.

[100] M. T. Nazir, B. T. Phung, Y. Zhang, and S. Li, "Dielectric and thermal properties of micro/nano boron nitride co-filled EPDM composites for high-voltage insulation," *Micro Nano Lett.*, vol. 14, no. 2, pp. 150–153, 2019.

[101] Q. Wang, X. Chen, C. Dai, A. Paramane, M. Awais, and N. Ren, "Experimental and finite element analysis of epoxy-based composites for packaging materials to reduce electric field and power loss under ac and dc conditions," *IEEE Trans. Compon. Packag. Manuf. Technol.*, vol. 12, no. 1, pp. 11–26, Jan. 2022.

[102] T. Yao, K. Chen, T. Shao, C. Zhang, C. Zhang, and Y. Yang, "Nano-BN encapsulated micro-AlN as fillers for epoxy composites with high thermal conductivity and sufficient dielectric breakdown strength," *IEEE Trans. Dielectr. Electr. Insul.*, vol. 27, no. 2, pp. 528–534, Apr. 2020.

[103] K. Mori, N. Hirai, Y. Ohki, Y. Otake, T. Umemoto, and H. Muto, "Effects of interaction between filler and resin on the glass transition and dielectric properties of epoxy resin nanocomposites," *IET Nanodielectrics*, vol. 2, no. 3, pp. 92–96, 2019.

[104] Y. Zhang, Y. Zhou, X. Zhu, C. Teng, T. Zhang, and D. Hu, "Electrical tree evolution of BN sheet/epoxy resin composites at high voltage frequencies," *IEEE Trans. Dielectr. Electr. Insul.*, vol. 29, no. 5, pp. 1991–1999, Oct. 2022.

[105] S. Jingxuan, X. Qing, L. Xiuquan, Z. Meiying, Z. Yahui, and L. Fangcheng, "Enhanced performance of aramid/epoxy composites by silane coupling treatment of fillers," *IEEE Trans. Dielectr. Electr. Insul.*, vol. 30, no. 3, pp. 911–919, Jun. 2023.

[106] S. K. Paul, S. Maur, S. Biswas, and A. K. Pradhan, "Review on thermal and electrical properties for condition assessment of epoxy nanocomposites by advanced techniques," *IEEE Trans. Dielectr. Electr. Insul.*, vol. 31, no. 1, pp. 230–245, Feb. 2024.

[107] H. Xu, Q. Bu, X. Shang, and Q. Zhang, "Influence of voltage frequency and filler content on breakdown characteristics of epoxy resin," in *Proc. IEEE 6th Int. Electr. Energy Conf. (CIEEC)*, 2023, pp. 3306–3311.

[108] S. Nakamura *et al.*, "Effects of temperature on electrical treeing and partial discharges in epoxy/silica nanocomposites," *IEEE Trans. Dielectr. Electr. Insul.*, vol. 27, no. 4, pp. 1169–1177, Aug. 2020.

[109] A. Shundo, S. Yamamoto, and K. Tanaka, "Network formation and physical properties of epoxy resins for future practical applications," *JACS Au*, vol. 2, no. 7, pp. 1522–1542, Jul. 2022.

[110] Y. Gong, W. Zhou, Y. Kou, L. Xu, H. Wu, and W. Zhao, "Heat conductive h-BN/CTPB/epoxy with enhanced dielectric properties for potential high-voltage applications," *High Volt.*, vol. 2, no. 3, pp. 172–178, 2017.

[111] L. Liu, D. Nam, B. Guo, J. Ewanchuk, R. Burgos, and G.-Q. Lu, "Glass for encapsulating high-temperature power modules," *IEEE J. Emerg. Sel. Top. Power Electron.*, vol. 9, no. 3, pp. 3725–3734, Jun. 2021.

[112] L. Liu, D. Nam, B. Guo, R. Burgos, and G. Lu, "Evaluation of a lead glass for encapsulating high-temperature power modules for aerospace application," in *Proc. Int. Tech. Conf. Exhib. Packag. Integr. Electron. Photonic Microsystems*, 2019.

[113] J. Chen, W. Chen, L. Zhang, X. Yan, J. Fan, and H. Zeng, "Tuning the thermal and insulation properties of bismuth borate glass for SiC power electronics packaging," *J. Am. Ceram. Soc.*, vol. 107, no. 4, pp. 2207–2216, 2024.

[114] T. D. Mekuria, L. Wang, C. Zhang, M. Yang, Q. Lv, and D. E. Fouad, "Synthesis and characterization of high strength polyimide/silicon nitride nanocomposites with enhanced thermal and hydrophobic properties," *Chin. J. Chem. Eng.*, vol. 32, pp. 446–453, Apr. 2021.

[115] H. Zhao *et al.*, "Electrical and mechanical properties of polyimide composite films reinforced by ultralong titanate nanotubes," *Surf. Coat. Technol.*, vol. 360, pp. 13–19, Feb. 2019.

[116] M. Chen, W. Zhou, J. Zhang, and Q. Chen, "Dielectric property and space charge behavior of polyimide/silicon nitride nanocomposite films," *Polymers*, vol. 12, no. 2, Art. no. 2, Feb. 2020.

[117] M. Zhang *et al.*, "Preparation and characterization of semi-alicyclic polyimides containing trifluoromethyl groups for optoelectronic application," *Polymers*, vol. 12, no. 7, Art. no. 7, Jul. 2020.

[118] H. Lao *et al.*, "Transparent polyamide-imide films with high *T*g and low coefficient of thermal expansion: Design and synthesis," *Polymer*, vol. 206, p. 122889, Oct. 2020.

[119] W. Chen, F. Liu, M. Ji, and S. Yang, "Synthesis and characterization of low-CTE polyimide films containing trifluoromethyl groups with water-repellant characteristics," *High Perform. Polym.*, vol. 29, no. 5, pp. 501–512, Jun. 2017.

[120] K. Ruan, Y. Guo, and J. Gu, "Liquid crystalline polyimide films with high intrinsic thermal conductivities and robust toughness," *Macromolecules*, vol. 54, no. 10, pp. 4934–4944, May 2021.

[121] A. Can-Ortiz, L. Laudebat, Z. Valdez-Nava, and S. Diaham, "Nonlinear electrical conduction in polymer composites for field grading in high-voltage applications: A review," *Polymers*, vol. 13, no. 9, Jan. 2021.

[122] M. Sato, A. Kumada, K. Hidaka, T. Yasuoka, Y. Hoshina, and M. Shiiki, "Multi-Scale modeling of dielectric polarization in polymer/ferroelectric composites," *IEEE Trans. Dielectr. Electr. Insul.*, vol. 30, no. 2, pp. 674–680, Apr. 2023.

[123] N. Wang, I. Cotton, J. Robertson, S. Follmann, K. Evans, and D. Newcombe, "Partial discharge control in a power electronic module using high permittivity non-linear dielectrics," *IEEE Trans. Dielectr. Electr. Insul.*, vol. 17, no. 4, pp. 1319–1326, Aug. 2010.

[124] B. R. Varlow, J. Robertson, and K. P. Donnelly, "Nonlinear fillers in electrical insulating materials," *IET Sci. Meas. Amp Technol.*, vol. 1, no. 2, pp. 96–102, Mar. 2007.

[125] J.-W. Zha, M.-S. Zheng, B.-H. Fan, and Z.-M. Dang, "Polymer-based dielectrics with high permittivity for electric energy storage: A review," *Nano Energy*, vol. 89, p. 106438, Nov. 2021.

[126] U. Waltrich, C. F. Bayer, M. Reger, A. Meyer, X. Tang, and A. Schletz, "Enhancement of the partial discharge inception voltage of ceramic substrates for power modules by trench coating," in *Proc. Int. Conf. on Electron. Packag. (ICEP)*, 2016, pp. 536–541.

[127] N. Hasan, N. H. Noordin, M. S. A. Karim, N. a. T. Yusof, and M. R. M. Rejab, "Epoxy-barium titanate nanocomposite fabrication process and dielectric properties at S and G band," pp. 238–243, Jan. 2022.

[128] A. Escriva *et al.*, "Thickness dependence of epoxy-based composites with batio$_3$ particles on AC electrical breakdown strength," in *Proc. IEEE 4th Int. Conf. Dielectr. (ICD)*, 2022, pp. 1-4.

[129] L. Zhong *et al.*, "An integrated structure–material optimization strategy for the packaging of high-voltage insulated gate bipolar transistors," *IEEE Trans. Dielectr. Electr. Insul.*, vol. 29, no. 6, pp. 2163–2170, Dec. 2022.

[130] F. Yan, L. Wang, H. Wang, S. Wang, and K. Gao, "High temperature characteristics of composite materials composed of silicone gel and barium titanate in high voltage power modules," *IEEE Trans. Ind. Appl.*, vol. 59, no. 3, pp. 3648–3659, May 2023.

[131] H. Wen, L. Cheng, Y. Jiang, T. Zhu, and Z. Chen, "Comparative study on thermal and electrical properties of EP/SrTiO3and EP/BaTiO3nanocomposites," in *Proc. IEEE Int. Conf. High Voltage Eng. and Appl. (ICHVE)*, 2020, pp. 1–4.

[132] G. Belijar *et al.*, "Dielectric breakdown of high-k epoxy-based anisotropic composites," in *Proc. IEEE Conf. Electr. Insul. Dielectr. Phenomenon (CEIDP)*, 2017, pp. 560–563.

[133] S. Diaham, Z. Valdez-Nava, L. Lévêque, T. T. Le, L. Laudebat, and T. Lebey, "Field grading composites tailored by electrophoresis — Part 1: Principle and permittivity gradient in uniform electric field," *IEEE Trans. Dielectr. Electr. Insul.*, vol. 28, no. 2, pp. 333–340, Apr. 2021.

[134] S. Diaham, Z. Valdez-Nava, T. T. Le, L. Lévêque, L. Laudebat, and T. Lebey, "Field grading composites tailored by electrophoresis—Part 2: permittivity gradient in non-uniform electric field," *IEEE Trans. Dielectr. Electr. Insul.*, vol. 28, no. 2, pp. 341–347, Apr. 2021.

[135] S. Diaham, Z. Valdez-Nava, T. T. Le, L. Lévêque, L. Laudebat, and T. Lebey, "Field grading composites tailored by electrophoresis—part 3: Application to power electronics modules encapsulation," *IEEE Trans. Dielectr. Electr. Insul.*, vol. 28, no. 2, pp. 348–354, Apr. 2021.

[136] M.-R. Halloum, B. S. Reddy, and G. N. Reddy, "Stress control for polymeric outdoor insulators using nonlinear resistive field grading materials operating under different conditions," *IEEE Trans. Dielectr. Electr. Insul.*, vol. 29, no. 3, pp. 1175–1182, Jun. 2022.

[137] X. Zhao *et al.*, "Grading of electric field distribution of AC polymeric outdoor insulators using field grading material," *IEEE Trans. Dielectr. Electr. Insul.*, vol. 26, no. 4, pp. 1253–1260, Aug. 2019.

[138] T. Christen, L. Donzel, and F. Greuter, "Nonlinear resistive electric field grading part 1: Theory and simulation," *IEEE Electr. Insul. Mag.*, vol. 26, no. 6, pp. 47–59, Nov. 2010.

[139] L. Donzel, F. Greuter, and T. Christen, "Nonlinear resistive electric field grading Part 2: Materials and applications," *IEEE Electr. Insul. Mag.*, vol. 27, no. 2, pp. 18–29, Mar. 2011.

[140] O. Faruqe, F. Haque, P. C. Saha, I. Jovanovic, N. Uzelac, and C. Park, "Partial incorporation of nonlinear resistive field grading materials: A strategy for enhanced field reduction and safety," *IEEE Trans. Dielectr. Electr. Insul.*, vol. 30, no. 1, pp. 474–483, Feb. 2023.

[141] L. Donzel and J. Schuderer, "Nonlinear resistive electric field control for power electronic modules," *IEEE Trans. Dielectr. Electr. Insul.*, vol. 19, no. 3, pp. 955–959, Jun. 2012.

[142] K. Li, B. Zhang, X. Li, F. Yan, and L. Wang, "Electric field mitigation in high-voltage high-power IGBT modules using nonlinear conductivity composites," *IEEE Trans. Compon. Packag. Manuf. Technol.*, vol. 11, no. 11, pp. 1844–1855, Nov. 2021.

[143] C. F. Bayer, U. Waltrich, A. Soueidan, E. Baer, and A. Schletz, "Partial discharges in ceramic substrates - correlation of electric field strength simulations with phase resolved partial discharge measurements," *Trans. Jpn. Inst. Electron. Packag.*, vol. 9, pp. E16-003-1-E16-003–009, 2016.

[144] M. M. Tousi and M. Ghassemi, "The effect of type of voltage (sinusoidal and square waveform) and the frequency on the performance of nonlinear field-dependent conductivity coatings for electric field control in power electronic modules," in *Proc. IEEE Conf. Electr. Insul. Dielectr. Phenomenon (CEIDP)*, 2019, pp. 552–555.

[145] M. M. Tousi and M. Ghassemi, "Nonlinear field dependent conductivity materials for electric field control within next-generation wide bandgap

power electronics modules," in *Proc. IEEE Electr. Insul. Conf. (EIC)*, 2019, pp. 63–66.
[146] J. Li, Y. Liang, Y. Mei, X. Tang, and G.-Q. Lu, "Packaging design of 15 kv SiC power devices with high-voltage encapsulation," *IEEE Trans. Dielectr. Electr. Insul.*, vol. 29, no. 1, pp. 47–53, Feb. 2022.
[147] Y. Liang, G. Zhu, G.-Q. Lu, and Y.-H. Mei, "Reliable epoxy/SiC composite insulation coating for high-voltage power packaging," *J. Mater. Sci. Mater. Electron.*, vol. 33, no. 26, pp. 20508–20517, Sep. 2022.
[148] Y. Dai, Y. Zhao, W. Yang, Y. Chen, and L. Wei, "Thermal stress analysis of epoxy resin encapsulated solid state transformer's cracking caused by temperature shock," in *Proc. Int. Conf. Electr. Mater. Power Equip. (ICEMPE)*, 2021, pp. 1–4.
[149] F. Azimpour-Shishevan, H. Akbulut, and M. A. Mohtadi-Bonab, "The effect of thermal shock cycling on low velocity impact behavior of carbon fiber reinforced epoxy composites," *J. Dyn. Behav. Mater.*, vol. 5, no. 2, pp. 161–169, Jun. 2019.
[150] K.-B. Sun, Y.-H. Mei, Z.-B. Shuai, and L. Li, "Insulation and reliability enhancement by a nonlinear conductive polymer-nanoparticle coating for packaging of high-voltage power devices," *IEEE Trans. Dielectr. Electr. Insul.*, vol. 30, no. 6, pp. 2514–2521, Dec. 2023.
[151] J. Xu, Z. Zhang, K. D. T. Ngo, and G.-Q. Lu, "Desired properties of a nonlinear resistive coating for shielding triple point in a medium-voltage power module," *IEEE Trans. Dielectr. Electr. Insul.*, vol. 28, no. 5, pp. 1721–1728, Oct. 2021.
[152] Y. Gao, Y. Yang, H. Zhao, T. S. Aunsborg, S. Munk-Nielsen, and C. Uhrenfeldt, "Analysis of nonlinear conductivity coating used to improve electric field distribution in medium voltage power module," in *Proc. IEEE Energy Convers. Congr. Expo (ECCE)*, 2022, pp. 1–7.
[153] X. Yang, X. Zhao, J. Hu, and J. He, "Grading electric field in high voltage insulation using composite materials," *IEEE Electr. Insul. Mag.*, vol. 34, no. 1, pp. 15–25, Jan. 2018.
[154] P. Adhikari and M. Ghassemi, "A review of insulation challenges and mitigation strategies in (U)WBG power modules packaging," in *Proc. IEEE Texas Power* and *Energy Conf. (TPEC)*, 2024.
[155] M. M. Tousi and M. Ghassemi, "Electric field control by nonlinear field dependent conductivity dielectrics characterization for high voltage power module packaging," in *Proc. IEEE Int. Workshop Integr. Power Packag. (IWIPP)*, 2019, pp. 54–58.
[156] M. M. Tousi and M. Ghassemi, "Influence of temperature and frequency on electric field reduction method via a nonlinear field dependent conductivity layer combined with protruding substrate for power electronics modules," in *Proc. IEEE Electr. Insul. Conf. (EIC)*, 2020, pp. 94–97.
[157] M. M. Tousi and M. Ghassemi, "Electrical insulation design and accurate estimation of temperature via an electrothermal model for a 10 kV SiC power module packaging," in *Proc. IEEE Conf. Electr. Insul. Dielectr. Phenomenon (CEIDP)*, 2020, pp. 407–410.
[158] M. M. Tousi and M. Ghassemi, "Characterization of nonlinear field-dependent conductivity layer coupled with protruding substrate to address high electric field issue within high-voltage high-density wide bandgap power modules," *IEEE J. Emerg. Sel. Top. Power Electron.*, vol. 8, no. 1, pp. 343–350, Mar. 2020.
[159] C. Lagomarsini, C. Jean-Mistral, A. Kachroudi, S. Monfray, and A. Sylvestre, "Outstanding performance of parylene polymers as electrets for energy harvesting and high-temperature applications," *J. Appl. Polym. Sci.*, vol. 137, no. 23, p. 48790, 2020.
[160] X. Li *et al.*, "Polymer electrets and their applications," *J. Appl. Polym. Sci.*, vol. 138, no. 19, p. 50406, 2021.
[161] C. Park, "Electret: an entirely new approach of solving partial discharge caused by triple points, sharp edges, bubbles, and airgaps," *IEEE Access*, vol. 8, pp. 78354–78366, 2020.

Pujan Adhikari (Graduate Student Member, IEEE) received a B.E. degree in electrical engineering from Tribhuvan University, Pulchowk Campus, Nepal, in 2022. He is currently pursuing a Ph.D. degree with the Department of Electrical and Computer Engineering at the University of Texas at Dallas.

His research interests include high-voltage engineering, electrical insulation materials and systems, Multiphysics modeling, and (ultra)wide bandgap power electronics packaging.

Mona Ghassemi (Senior Member, IEEE) received the Ph.D. degree (First Hons.) in electrical engineering from the University of Tehran, Tehran, in 2012. From 2013 to 2015, she was a Postdoctoral Fellow with NSERC/ Hydro-Québec/UQAC Industrial Chair on Atmospheric Icing of Power Network Equipment (CIGELE), University of Québec at Chicoutimi (UQAC), Chicoutimi, QC, Canada. She has been a Registered Professional Engineer, since 2015. She was also a Postdoctoral Fellow with the University of Connecticut, Storrs, CT, USA, from 2015 to 2017. In 2017, she joined the Bradley Department of Electrical and Computer Engineering, Virginia Tech, Blacksburg, VA, USA, as an Assistant Professor. In 2021, she was named both the Steven O. Lane Junior Faculty Fellow and the College of Engineering Faculty Fellow of Virginia Tech. In 2022, she joined the Department of Electrical and Computer Engineering, The University of Texas at Dallas, as an Associate Professor with tenure (early tenure), and the Chairholder of Texas Instruments Early Career Award, from 2022 to 2028. She has authored more than 160 peer-reviewed journal and conference papers and one book chapter. Her research interests include electrical insulation materials and systems, high voltage/field engineering and technology, power systems, and plasma science.

Dr. Ghassemi was a member of the Nominations and Appointments Committee of the IEEE Dielectrics and Electrical Insulation Society (DEIS). She is currently the At-Large Member of the Administrative Committee of the IEEE DEIS, a DEIS Representative of the IEEE USA Public Policy Committee on Transportation and Aerospace Policy (CTAP) and USA Technology Policy Council Research and Development Policy Committee, a Corresponding Member of the IEEE Conference Publication Committee (CPC) of the IEEE Power and Energy Society (PES), an Active Member of several CIGRE working groups and the IEEE Task Forces, a DEIS Technical Committee Member on Dielectrics and Electrical Insulation for Transportation Electrification, and a member of the Education Committee of IEEE DEIS and PES. She received the three most prestigious and most competitive career awards, which are the 2021 Department of Energy (DOE) Early Career Research Program Award, the 2020 National Science Foundation (NSF) CAREER Award, and the 2020 Air Force Office of Scientific Research (AFOSR) Young Investigator Research Program (YIP) Award. She received the 2020 Contribution Award from *IET High Voltage* and also received four best paper awards. She is the Vice-President (Technical) of IEEE DEIS. She is an Associate Editor of IEEE TRANSACTIONS ON DIELECTRICS AND ELECTRICAL INSULATION, IEEE TRANSACTIONS ON INDUSTRY APPLICATIONS, *IET High Voltage*, *International Journal of Electrical Engineering Education*, and *Power Electronic Devices and Components*, and a Guest Editor of *Aerospace* and *Energies*.